CHAPTER 5

HETEROHEDRAL METALLOFULLERENES

Heterohedral metallofullerenes, fullerenes with metals in the carbon network, are less common and have been studied less than the other members of the metallofullerene family: the endohedral (Chapter 4) and the exohedral (Chapter 6). The term heterofullerenes will be used as an abbreviation of heterohedral metallofullerenes. Also, the mono- and di- prefixes before heterofullerenes will indicate the number of metals incorporated into the fullerene carbon framework.

Although nitrogen and boron atoms are common as doped atoms in C_{60} and C_{70} fullerenes and give a formidable range of stoichiometries, the chemical art of incorporating metals by replacing one or two carbons is still in its infancy. Branz's and Balch's groups were the first experimentalists to detect this kind of metallofullerenes. Heterohedral metallofullerenes are detected by mass spectra studies, but the synthesis of bulky quantities and the use of spectrometric techniques have yet to be reported. The new heterohedral metallofullerenes have the following four stoichiometries: (1) monoheterofullerenes in which one carbon is replaced by one metal: $C_{59-2x}M$ and $C_{69-2x}M$ (x = 0, 1, 2; M = Si, Fe, Co, Ni, Rh, Pt, Ir, Sm, Ni, La, Y, Rh) — x = 1 and 2 are obtained from x = 0 stoichiometry by successive losses of C_2 units — (2) monoheterofullerenes in which a C_2 unit is replaced by single metal: $C_{58}M$ (M = Pt, Ir); (3) diheterofullerenes in which one C atom and a C_2 unit are replaced by two metals: $C_{57}Pt_2$ and finally (4) diheterofullerenes in which two C_2 units are replaced, $C_{56}Pt_2$.

The present chapter starts by presenting the limited experimental studies and some theoretical advances made in the comprehension of the electronic structure of these new metallofullerenes (section 5.1). The encapsulation of Sc_3N inside the C_{68}, C_{78} and C_{80} provided us with a good clear example of an ionic bond between two units. However, in heterohedral fullerenes the metal bond in the fullerene carbon framework does not seem as easy to rationalize as in the TNT endohedral metallofullerenes. The metal is incorporated in the carbon network of the fullerene as another atom and does not disrupt the rest. To date no studies have dealt with how the metals are bonded to the other carbons. Bora- and azafullerenes can not be taken as suitable models because they have only slight electronic variations from the original carbon. The metal bond will be exemplified by the simplest monoheterofullerene: $C_{58}Pt$ (section 5.2). In order to understand how the metal is incorporated into the fullerene carbon framework two tools are mainly used: (1) the decomposition of the substitution energy, and (2) the fragment molecular orbital method applied to the analogous $C_{24}H_{12}Pt$ compound. Then the isomerism, and the geometric and electronic structures of the monoheterofullerenes: $C_{58}M$ and $C_{59}M$ (M = Pt, Ir, Os, Ti) are systematically studied in section 5.3. The experimental evidence for the ability of $C_{59}M$ and $C_{58}M$ (M = Pt, Ir) to bind to olefins is studied in the next section 5.4. In section 5.5, we present the huge theoretical study on the $C_{56}Pt_2$ and $C_{57}Pt_2$ diheterofullerenes. The substitution of two C_2 units or one C_2 unit and one C atom in C_{60} yields a very high number of regioisomers, which makes the theoretical analysis of the dimetallic species much more complicated. We report a detailed DFT study on the factors that govern the relative stability of the regioisomers of $C_{56}Pt_2$ and $C_{57}Pt_2$. Because of the numerous factors affecting the stability, we were forced to use chemometric techniques. Finally in section 5.6, these heterofullerenes are characterized by the calculation of the ionization potentials and the electron affinities.

5.1 INTRODUCTION 157
5.1.1 Experimental part 157
5.1.2 Theoretical part..... 158

5.2 COVALENT METAL BOND IN THE FULLERENE CARBON FRAMEWORK 159
5.2.1 Geometric and electronic structure of $C_{58}Pt$ 159
5.2.2 Substitution energy (SE) and its decomposition 161
5.2.3 Hole energy, ΔE_{HOLE} 164
5.2.4 Insertion binding energy (IBE) 164
5.2.5 Fragment molecular orbital method 165

5.3 MONOHETEROFULLERENES: $C_{58}M$, $C_{59}M$ (M = Pt, Ir, Os, Ti) and $C_{68}Pt$ 174
5.3.1 $C_{58}M$ (M = Pt, Ir, Os, Ti) 174
5.3.2 $C_{68}Pt$, a doped fullerene from D_{5h}-C_{70} 178
5.3.3 $C_{59}M$ (M = Pt, Ir, Os, Ti) 180
5.3.4 Stability of neutral monoheterofullerenes versus cation and anion analogues 183

5.4 ADDITON OF ETHYLENE TO MONOHETEROFULLERENES 184
5.4.1 Experimental evidence 184
5.4.2 Interaction between ethylene and monoheterofullerenes 185

5.5 DIHETEROFULLERENES: $C_{57}Pt_2$, $C_{56}Pt_2$ and $C_{81}Pt_2$ 192
5.5.1 Regioisomers of $C_{57}Pt_2$ 193
5.5.2 Regioisomers of $C_{56}Pt_2$ 197
5.5.3 Electronic structure 200
5.5.4 Metal-metal coupling 202
5.5.5 Topological and structural factors that govern isomer stability 205
5.5.6 Chemometric study of the structure-energy relationship 211

5.5.7 Stability of the carbon skeleton is the principal factor that determines the isomer stability ……..……..……. 215
*5.5.8 Prediction of isomer stability of $C_{81}Pt_2$, a doped fullerene from D_{2d}-(C_{84}:**23**)* ……..……. 218

5.6 PHYSICAL PROPERTIES …… 222

5.7 CONCLUDING REMARKS ……..……. 223

REFERENCES AND NOTES ……...… 228

5.1 INTRODUCTION

5.1.1 Experimental part

The macroscopic synthetic methods that have been developed for azafullerenes and borafullerenes of C_{60} and C_{70} since 1995 have led to a whole new rich area in the science of fullerenes: cage modification chemistry. Heterohedral non-metallofullerenes have been synthesized using a modified Krätschmer-Huffman process.[1] Moreover, the fact that these compounds are numerous has also led to a wide variety of studies on the characterization and determination of their physicochemical properties. Heterohedral metallofullerenes, on the other side, have appeared very recently in fullerene chemistry. Without a doubt, this area is in its infancy because only mass spectrometric studies have been made up to now, not characterization or spectrometric studies. However, these new heterohedral fullerenes are expected to increase rapidly when ways of producing them in significant quantities are discovered.

Mass spectrometric studies have identified a number of fullerene-like clusters with heteroatoms incorporated into the fullerene carbon framework. First, Jarrold and coworkers demonstrated that NbC_x^+ clusters could be generated by pulsed laser vaporization of graphite/NbC composites and that the mobilities of the NbC_x^+ clusters indicated that those with odd values of x contained Nb atoms that resided on the surface.[2] Related clusters could also be formed by substitution-like processes that use preformed fullerene cages. For example, Branz and co-workers prepared the gas phase clusters $C_{60}M_x$ and $C_{70}M_x$ by evaporating of the metal (M) into the fullerene vapor.[3,4] Subsequent photo fragmentation of $C_{60}M_x$ and $C_{70}M_x$ produces new clusters with the compositions $C_{59-2x}M$ and $C_{69-x}M$ with M = Si, Fe, Co, Ni, Rh, Ir and x = 0, 1, 2. As demonstrated in Balch's laboratories, an alternative route to the formation of the clusters $C_{59-2x}M^+$ and $C_{69-x}M^+$ involves laser ablation of electrochemically deposited films (C_{60}/Pt or C_{60}/Ir(CO)$_2$) that contain polymeric, covalently bound chains: ...$C_{60}ML_xC_{60}ML_xC_{60}ML_x$..., where ML_x = Ir(CO)$_2$ or Pt.[5,6,7] This process extended to form related clusters involving Sm, Ni, La, Y, and Rh.[8] In the negative ion mode, the C_{60}/Pt film produces, among other species, the ion $C_{58}Pt^-$ —the result of the substitution of two C atoms for a Pt atom — and

the ions $C_{57}Pt_2^-$ and $C_{56}Pt_2^-$, which incorporate two Pt atoms into the cage. The $C_{60}/Ir(CO)_2$ film produces a different series of products: $C_{59}Ir^-$, $C_{58}Ir^-$, $C_{57}Ir^-$ and $C_{56}Ir^-$, in which an iridium atom can also replace one or two carbons within the fullerene cage. On the other hand, evidence for the ability of the metals in some of these fullerenes to bind additional ligands was obtained by conducting the laser ablation studies in the presence of 2-butene where adducts such as $[C_{59}Ir(2\text{-butene})]^-$, $[C_{58}Ir(2\text{-butene})]^-$, $[C_{57}Ir(2\text{-butene})]^-$ and $[C_{56}Ir(2\text{-butene})]^-$ were observed.[9] The results of laser ablation studies of the electrochemically deposited $C_{60}\{Ir(CO)_2\}_n$ film in positive ion mode revealed the presence of $C_{59}Ir^+$ and $C_{57}Ir^+$. The spectral features of the formation of $C_{69}Ir^+$ were obtained by desorption from a film prepared by electrochemical reduction of a solution of C_{70} and $Ir(CO)_2Cl(NH_2C_6H_4Me\text{-}p)$. Finally, $C_{59}Pt^+$ was obtained by desorption from a film of $C_{60}Pt_n$ prepared by electrochemical reduction of a solution of C_{60} and $PtCl_2(pyridine)_2$.

5.1.2 Theoretical part

As far as theory is concerned, semiempirical methods have been used to study regioisomerism for nitrogen and boron doped fullerenes[10,11,12] and other atoms such as oxygen, sulfur[13] and aluminum.[14] The development of the heterofullerene isomerism can be seen in a recent paper by Jiao et al., which contains the latest literature on semiempirical methods.[15] Density functional theory (DFT) based calculations have been performed to study the structure and the electronic properties of the $C_{59}M$ (M = Si,[16] Pt, Ir, Fe, Co, Ni, Rh[17]) and $C_{69}M$ (M = Co, Rh, Ir)[18] monoheterofullerenes. Although Si is not a transition-metal atom, it is interesting how this atom replaces carbons because it is a larger dopant than nitrogen and boron. Its effect, then, can be easily compared to that of a transition-metal atom. The replacement of two single carbons by two Si atoms in C_{60} led to $C_{58}Si_2$. The structure of this fullerene turns out to be modified only in the vicinity of the dopant atoms, and the Si–C distances are as much as 30% longer that the C–C distances. The $C_{58}Si_2$ compound is more stable when the Si atoms are rather close, 3.47 Å. DFT studies of $C_{59}Pt$ and $C_{59}Ir$ showed that the metals are found in three coordinated sites on the fullerene surface. Because the Ir–C or Pt–C bond lengths are longer than the C–C bond lengths, the Ir or Pt

atoms protrude from the fullerene surface. The theoretical work has also indicated that the addition of a ligand to the exposed metal would be energetically favorable. Studies of $C_{59}Fe$ revealed a similar structure.[19] The electronic structure of $C_{59}M$ varies with the M and can be described in terms of defect levels in the free fullerene host, C_{60}. Computational studies of $C_{69}M$ structures, where M = Co, Rh, and Ir, demonstrated that substitution at the more highly pyramidalized poles of the fullerene was energetically favored. Recently DFT calculations have been performed to determine the structure of the heterohedral metallofullerenes: $C_{53}Rh$ and $C_{54}M$ (M = Rh, Y). They belong to the group of $C_{2x+1}M$ and $C_{2x}M$ (M = Rh, Y) heterohedral and endohedral metallofullerenes obtained from a laser ablation of $C_{60}M_n$ (M = Rh, Y) metal fullerides.[20]

5.2 COVALENT METAL BOND IN THE FULLERENE CARBON FRAMEWORK

5.2.1 Geometric and electronic structure of $C_{58}Pt$

Substitution of a C_2 unit for a metal in C_{60} results in the formation of two different isomers, because the C_2 unit can be removed from a 6:6 or a 6:5 ring junction. Hereafter, the resulting structures will be referred to as C_{2v}-$C_{58}Pt$ and C_s-$C_{58}Pt$, respectively, according to their symmetry. Figure 5.1 shows drawings of the optimal structures of $C_{58}M$ isomers. They are compared to the $C_{59}M$ structure, in which only one carbon is replaced by a metal. Table 5.1 collates the geometric properties and Mulliken net charges for the monoheterofullerenes $C_{58}Pt$ and $C_{59}Pt$. C_{2v}-$C_{58}Pt$ possesses four equivalent Pt–C distances equal to 2.034 Å but C_s-$C_{58}Pt$ possesses two lower distances of 2.013 Å between Pt and the hexagonal C atoms and two higher distances of 2.049 Å between Pt and the pentagonal C atoms. As can be seen in Figure 5.1, the four-coordinated metals in both isomers of $C_{58}Pt$ do not protrude from the fullerene surface but stay within the fullerene carbon framework. In contrast, the three-coordinated metal in $C_{59}M$ bulges out from the fullerene surface.

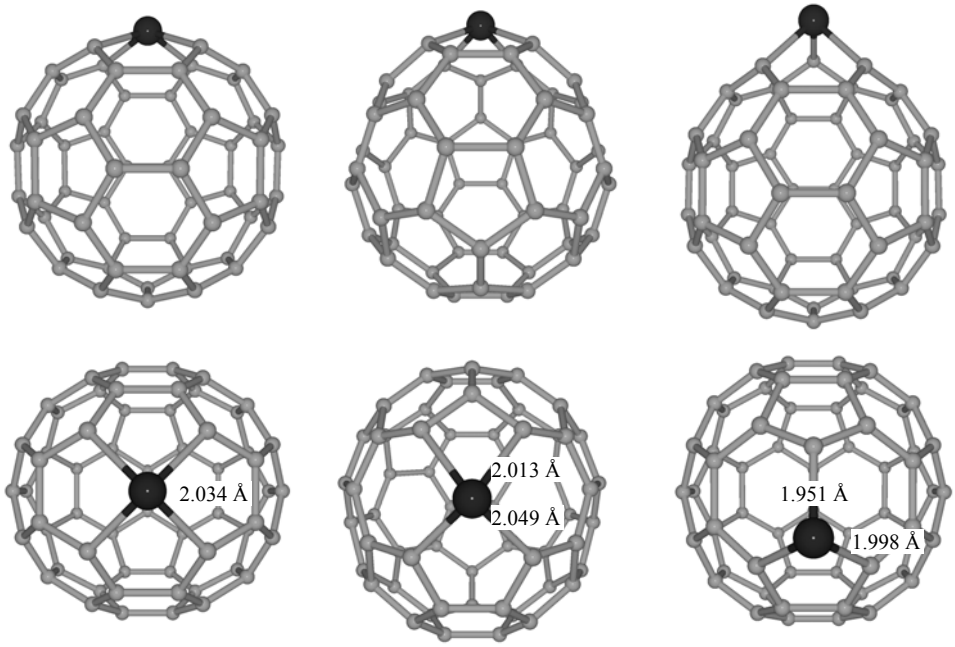

Figure 5.1 Two perspective visions of the C_{2v}-C_{58}Pt (a) (substitution at 6:6 C–C bond) and C_s-C_{58}Pt (b) (substitution at 6:5 C–C bond) isomers. For comparison the figure also includes the structure of C_{59}M (c). All Pt–C distances are shown for each heterofullerene.

C_{2v}-C_{58}Pt is the most stable isomer, 0.63 eV lower in energy than the C_s-C_{58}Pt isomer. Mulliken population analysis of the most stable isomer indicates that the electron charge transfer takes place from the metal to the carbon cage in C_{58}Pt. The net charge on the metal center is +0.82 *e*, and the negative charge on the carbons bonded to Pt is –0.37 *e*. The other carbons have smaller charges. The electronic populations of the *s*, *p* and *d* Pt orbitals are 2.590, 6.385 and 8.201 *e*, respectively. These values are quite similar to the electronic populations of the corresponding orbitals in C_{59}Pt: 2.547, 6.313 and 8.385 *e*. The Voronoi partition scheme of the electron density suggests that the electron charge transfer is higher, since it gives a net charge of +1.46 *e* for the metal center and of –0.39 *e* for the carbons connected to Pt.

Table 5.1 Geometric and electronic properties for $C_{59}Pt$, C_{2v}-$C_{58}Pt$, C_s-$C_{58}Pt$ and $C_{24}H_{12}Pt$. The $C_{24}H_{12}Pt$ doped molecule will be used as a metal-carbon bond model for heterofullerenes [a]

Molecule	*Symmetry*	*Cage radius* [b]	*Pt–C Bond lengths* [c]	*Mulliken Net Charge*	
				M	C [c]
$C_{59}Pt$	Cs	3.580	1.998/1.951	0.755	–0.344
$C_{58}Pt$	C_{2v}	3.562	2.034	0.824	–0.367
$C_{58}Pt$	C_s	3.569	2.049/2.013	0.843	–0.361
$C_{24}H_{12}Pt$	D_{4h}	--	1.929	1.312	–0.228

[a] Distances in Å. [b] Cage radius is defined as the average distance of all surface atoms to the center of the fullerene. Cage radius for C_{60} is 3.551 Å. [c] Average values for the carbons bonded to the metal.

5.2.2 Substitution energy (SE) and their decomposition

The relative stability of the various monoheterofullerenes is evaluated through the substitution energy (SE). This energy corresponds to the energy process of the substitution of carbon units by metals. The processes are $C_{60} + M \rightarrow C_{59}M + C$ for $C_{59}M$ and $C_{60} + M \rightarrow C_{58}M + C_2$ for $C_{58}M$. Substitution of a 6:6 C_2 unit in C_{60} by a Pt atom requires a considerable amount of energy, 7.35 eV, and even slightly more when the Pt heteroatom replaces a 6:5 C_2 unit, 7.98 eV. Hence, the C_{2v} isomer is more stable than the C_s isomer by 0.63 eV. SE can be decomposed into several energies, each one of which provides clues about how metal is incorporated into the fullerene carbon framework. This decomposition also makes it possible to rationalize the different isomer stabilities of $C_{58}Pt$ and the insertion of different metals into the $C_{58}M$ structure. First we divide SE into two main parts:

(5.1) $$SE = \Delta E_{HOLE} + IBE$$

Table 5.2 Decomposition of the substitution energy (SE) for C_{2v}-$C_{58}Pt$ and C_s-$C_{58}Pt$ and D_{4h}-$C_{24}H_{12}Pt$ [a]

Carbon structure			C_{60}	C_{60}	$C_{26}H_{12}$
Doped structure			$C_{58}Pt$	$C_{58}Pt$	$C_{24}H_{12}Pt$
Symmetry			C_{2v}	C_s	D_{4h}
ΔE_{HOLE} [b]			17.90	19.31	16.92
IBE [c]	ΔE_{DE} [d]	$C_{58}/C_{24}H_{12}$	1.80	1.63	2.94
		C_2	–0.57	–0.98	–0.12
		M	0.49	0.49	0.49
		Total	1.72	1.14	3.31
	ΔE_{INT} [e]	ΔE_{ST}	18.11	16.15	28.49
		ΔE_{ORB}	–30.38	–28.62	–37.00
		Total	–12.27	–12.47	–8.51
	Total		–10.55	–11.33	–5.20
SE			7.35	7.98	11.72

[a] Energies in eV. The Substitution Energy (SE) is defined as the energy reaction of the process C_{60} + M → $C_{58}M$ + C_2 for $C_{58}M$ -and $C_{26}H_{12}$ + M→ $C_{24}H_{12}M$ + C_2 for $C_{24}H_{12}M$. This energy can be diveded into several contributions SE = ΔE_{HOLE} + IBE. [b] ΔE_{HOLE}, hole energy, accounts for the energy reaction of the process $C_{60} \rightarrow C_{58}^* + C_2^*$ and $C_{26}H_{12} \rightarrow C_{24}H_{12}^* + C_2^*$. C_{58}^* is calculated at the most stable electronic state (singlet) with the fixed geometry of free C_{60}. For the model, $C_{24}H_{12}^*$ is calculated as a triplet with the fixed geometry of $C_{26}H_{12}$. C_2* keeps the electronic configuration as its free C_2 analogue but the C–C distance from their precursor (C_{60} or $C_{26}H_{12}$). [c] IBE (insertion binding energy) account for the energy reaction of the process $C_{58}^* + C_2^* + M \rightarrow C_{58}M + C_2$ and $C_{24}H_{12}^* + C_2^* + M \rightarrow C_{24}H_{12}M + C_2$. IBE = ΔE_{DE} + ΔE_{INT}. [d] ΔE_{DE} accounts for the deformation energy for the fragments: $C_{58}^* \rightarrow C_{58}$, $C_{24}H_{12}^* \rightarrow C_{24}H_{12}$, $C_2^* \rightarrow C_2$ and M → M*. Where C_{58} with the fixed geometry found in $C_{58}Pt$, also $C_{24}H_{12}$ with the fixed geometry found in $C_{24}H_{12}Pt$ and C_2 optimised. The most stable electronic state for that holed carbon systems are triplet for both C_{58} and $C_{24}H_{12}$. M is calculated at the most stable electronic state (unrestricted). [e] Finally ΔE_{INT} accounts for the interaction energy between the fragments C_{58} and M* at the fixed $C_{58}M$ geometry or $C_{24}H_{12}$ and M* at the $C_{24}H_{12}M$ geometry. M* is calculated as a restricted electronic state while C_{58} and $C_{24}H_{12}$ are triplet according to previous comments.

The hole energy, ΔE_{HOLE}, is the energy necessary to make a hole in the free C_{60} fullerene. The binding energy (BE) between the hole and the metal for constructing the final structure of $C_{58}Pt$ is included in the insertion bonding energy (IBE). More details about the intricacies of these energies are given in the footnote of Table 5.2. The bond between the holed C_{58} fullerene and the M atom unit is also analyzed using the extended transition method

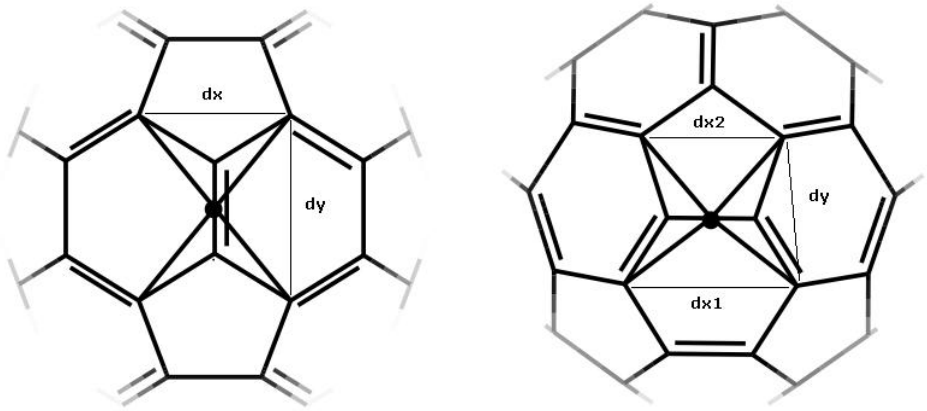

(a) substituted 6:6 C–C in C_{2v}-C_{58}M (b) Substituted 6:5 C–C in C_s-C_{58}M

Figure 5.2 Differences between the substitution of a pyracylene 6:6 C–C bond (a) and a corannulene 6:5 C–C bond (b) for a Pt atom in C_{60}. The formation of C_{2v}-C_{58}M requires the lost of 4 σ C–C bonds whereas the formation of C_s-C_{58}M a bit more: the lost of 4 σ and 2 π C–C bonds. Examples for d_x and d_y distances: d_x = 2.349 Å and d_y = 2.848 Å (in C_{2v}-C_{58} with C_{60} geometry), d_x = 2.657 Å and d_y = 2.665 Å (in C_{2v}-C_{58} with C_{2v}-C_{58}Pt geometry), d_{x2}/d_{x1} = 2.350/2.850 Å and d_y = 2.468 Å (C_s-C_{58} with C_{60} geometry) and d_{x2}/d_{x1} = 2.246/2.668 Å and d_y = 2.938 Å (in C_s-C_{58} with C_s-C_{58}Pt geometry).

developed by Ziegler and Rouk,[21] which is an extension of the well-known decomposition scheme of Morokuma.[22] According to this method, the IBE between two fragments can be decomposed into several contributions:

(5.2) $$IBE = \Delta E_{DE} + \Delta E_{ST} + \Delta E_{ORB}$$

More details about this decomposition can be found in subsection 4.2.4. The sum, $\Delta E_{ST} + \Delta E_{ORB}$, is known as the fragment interaction energy and represented by ΔE_{INT}. The values of this decomposition for both isomers of C_{58}Pt heterofullerene are shown in Table 5.2.

5.2.3 Hole energy, ΔE_{HOLE}

The process of making a hole is highly endothermic. The reaction $C_{60} \rightarrow C_{58} + C_2$ requires 17.90 eV when a 6:6 C_2 unit is removed and a little more is required, 19.31 eV, in the case of a 6:5 C_2 unit. In other words, the holed C_{58} fullerene is 1.41 eV more stable when the hole originates in a pyracylene C–C bond type than in a corannulene type. In the first step, C_{58} and C_2 keep the geometry which they had in the free C_{60} fullerene. The electronic state of a fullerene with a hole is not easy to determine because of the presence of dangling bonds. However, we found that the most stable electronic state of a holed C_{58} fullerene is a singlet independently of the type of hole. The triplet state is found to be 0.74 and 0.34 eV higher in energy for C_{2v}-C_{58} and C_s-C_{58}, respectively. The number of broken C–C bonds gives us some idea of the nature of the difference in the ΔE_{HOLE} between both holed C_{58} isomers. Unlike the most stable C_{2v}-C_{58} in which only four σ C–C bonds were broken, in the least stable C_s-C_{58} two additional π C–C bonds were also removed (see Figure 5.2 for clarification). ΔE_{HOLE} is the significant energy for determining the final value of SE, and hence for determining the most stable $C_{58}M$ isomer. In contrast, IBE is computed to be slightly more favorable in C_s-C_{58} by only 0.78 eV than in C_{2v}-C_{58}.

5.2.4 Insertion binding energy (IBE)

IBE is an exothermic process which helps monoheterofullerene formation. The first term of IBE, ΔE_{DE}, accounts for the energy necessary to convert C_2 and C_{58} fragments from their geometry and electronic state in the free C_{60} to their final forms: optimized C_2 and C_{58} with a $C_{58}M$ geometry, respectively. The electronic state of holed fullerenes is very sensitive to geometric changes. This is why the holed C_{58} fullerene with $C_{58}Pt$ geometry (either the C_{2v} or C_s isomer) has a triplet as the most stable electronic state, instead of the singlet shown in C_{58} with C_{60} geometry. The triplet is 0.35 eV and 0.26 eV stabilized above the singlet electronic state for holed C_{58} fullerenes with C_{2v}-$C_{58}Pt$ and C_s-$C_{58}Pt$ geometries, respectively. The dependence of the electronic state on the geometry deserves further discussion and will be dealt with in the next section.

In general, the deformation of the C_{58} core, $\Delta E_{DE}(C_{58})$, is very small and is restricted to the carbons directly linked to the metal. It is slightly higher for the C_{2v} isomer than for the C_s isomer, 1.80 and 1.63 eV, respectively. These differences in $\Delta E_{DE}(C_{58})$ between the C_s and C_{2v} isomers of $C_{58}Pt$ will also follow the same trend and magnitude for other analogue monoheterofullerenes: $C_{58}M$ (M = Ir, Os). The total ΔE_{DE} was computed to be 1.72 eV and 1.14 eV for C_{2v}-$C_{58}Pt$ and C_s-$C_{58}Pt$, respectively.

However, IBE is dominated by the ΔE_{INT}, and in particular by ΔE_{ORB}, because of favorable exothermic orbital interactions between both fragments and a lower repulsive ΔE_{ST} term. The ΔE_{ST} is related to the Pauli repulsion and the classical electrostatic interaction, but dominated by the former. So, the Pt–C distances and the space available in each hole to make the metal-carbon bond will be decisive in ΔE_{ST}. This space can be calculated as the delimited area by the four dangling C atoms: 6.690 $Å^2$ for the 6:6 hole and a little higher, 7.200 $Å^2$, for the 6:5 hole. These magnitudes confirm that the repulsion in the ΔE_{ST} term when the Pt metal is incorporated in the 6:6 hole, 18.11 eV, is higher than in the 6:5 hole, 16.15 eV. The computed exothermic values for the orbital term (ΔE_{ORB}) are high: –30.38 eV for C_{2v}-$C_{58}Pt$ and –28.81 eV for C_s-$C_{58}Pt$. They exemplify that when two neutral fragments are joined there is considerable electronic reorganization. The IBE, after ΔE_{DE}, ΔE_{ST} and ΔE_{ORB} are calculated, is clearly favorable to the C_s-$C_{58}Pt$ isomer by 0.78 eV. However, this is not enough to compensate for the more favorable stability (by 1.41 eV) of the ΔE_{HOLE} for the C_{2v}-$C_{58}Pt$ isomer. The IBE can be easily understood from the electronic structure of both isomers. Unlike C_{2v}-C_{58} which has only four dangling sp^2 electrons, the C_s-C_{58} isomer has two additional dangling p_z electrons, which means that the latter can interact more efficiently than the former.

5.2.5 Fragment molecular orbital analysis

In order to investigate how the metal is incorporated into the carbon framework, we analyzed the interaction orbital diagram between the two fragments: Pt and C_{58}. Albright made an in-depth study of orbitals in organometallic compounds.[23] The main idea is that the important valence orbitals of a molecule can be constructed from the valence orbitals of its

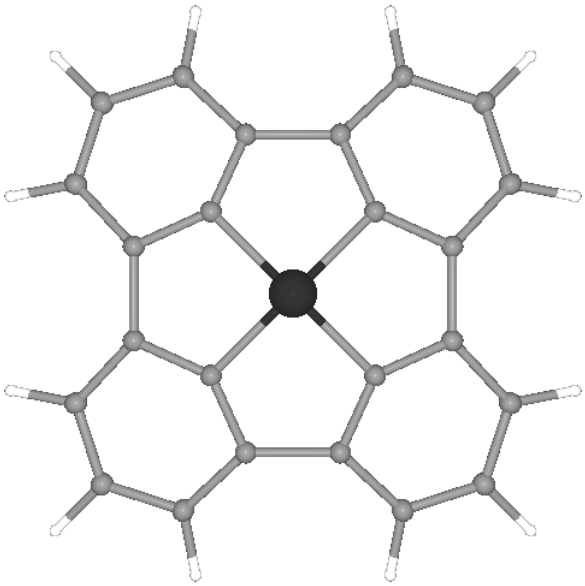

Figure 5.3 Optimized structure for D_{4h}-$C_{24}H_{12}Pt$, used as a bonding model for C_{2v}-$C_{58}Pt$.

constituent fragments. This method is another approach to, and a development of, the IBE described in above section.

The most stable diamagnetic organometallic compounds have a total of 18 electrons around the transition metal. In other words, there should be a total of 18 *d* metal electrons and electrons formally assigned to coordinate bonds from the surrounding ligands. In our specific case, the first fragment, the Pt atom, has 10 *d*-based valence electrons ($3d^9\ 4s^1\ 4p^0$) and the second fragment, the holed C_{2v}-C_{58} fullerene, has 4 σ-sp^2 electrons and 4 π-p_z electrons from the four dangling carbons. In conclusion, 18 electrons are involved in the metal-carbon bond. Therefore, Pt is formally in the 0 oxidation state.

Initially we used the planar D_{4h}-$C_{24}H_{12}Pt$ system in an attempt to explain the metal-carbon bond in the most symmetric C_{2v}-$C_{58}M$ isomer. Figure 5.3 shows the optimized structure of this compound. The substitution of the central 6:6 C–C bond in the polycyclic aromatic $C_{26}H_{12}$ compound leads to the planar D_{4h}-$C_{24}H_{12}Pt$ structure in which the Pt atom is tetra-tetracoordinated. This coordination can be taken as a model insertion because Pt incorporation into the fullerene carbon framework can be

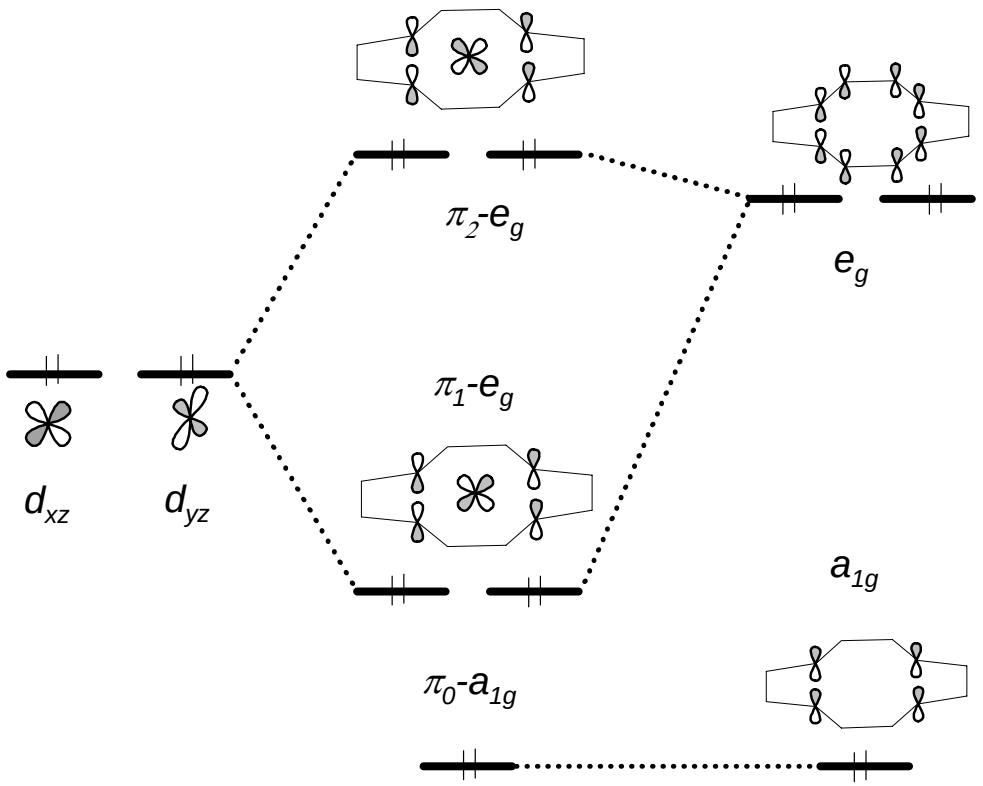

Figure 5.4 Molecular orbital (MO) correlation diagram for π interaction system between Pt (left, 4 *d* electrons in two metal orbitals) and $C_{24}H_{12}$ (right, 4 p_z electrons + 2 additional electrons in three carbon ligand orbitals) for the D_{4h}-$C_{26}H_{12}Pt$.

expected as a local interaction between the metal and the four dangling carbons. The most important distances and the decomposition of SE for this heterocompound have also been added to Table 5.1 and 5.2.

As is to be expected, the SE is clearly higher than the SE for heterofullerenes. When the C_2 unit is substituted by a Pt atom an energy of +11.72 eV is required. The $C_{26}H_{12}$ compound is highly aromatic and changes in the carbon skeleton will have a dramatic effect on their stability. So although it has fewer carbons the ΔE_{HOLE} is computed to be +16.92 eV. The insertion of Pt in this planar structure is also favorable but less than we expected (–5.20 eV for IBE). The expected high value for the ΔE_{ORB}

(–37.00 eV) is considerably compensated for by the ΔE_{DE} (3.31 eV) and the unexpected repulsive value of ΔE_{ST} (+28.49 eV). The repulsive value is probably due to the short Pt–C distance of 1.929 Å. The planar D_{4h}-$C_{24}H_{12}Pt$ heterocompound is a simplification of the C_{2v}-$C_{58}Pt$ metallofullerene but it is a suitable and powerful model for understanding the metal bond in the metallofullerene because: (1) all distances between close dangling carbons are equal and (2) the σ/π interactions are completely separable. The metal bond established in the D_{4h}-$C_{24}H_{12}Pt$ heterocompound will be explained through two independent molecular orbital correlation diagrams: one for the σ ligands (sp^2 carbon electrons) and the other for the π ligands (p_z carbon electrons). The knowledge acquired for the D_{4h}-$C_{24}H_{12}Pt$ heterocompound will be used to construct the metal bonds in C_{4v}-$C_{24}H_{12}Pt$ and C_{2v}-$C_{24}H_{12}Pt$, which are closer to those found in C_{2v}-$C_{58}Pt$.

Model MOs of D_{4h}-$C_{24}H_{12}Pt$. The π diagram is shown in Figure 5.4. The e_g and a_{1g} carbon ligand orbitals on the right hand side of the diagram represent the four π-p_z atomic orbitals of the four dangling carbons. It is important to notice that although the e_g orbital should be half filled, it is in fact completely filled because the four π-p_z electrons form π adjacent C–C bonds. The e_g ligand orbital matches the d_{xz} and d_{yz} metal orbitals and gives the bonding interaction π_1-e_g molecular orbital (MO) and the antibonding π_2-e_g MO. The a_{1g} ligand orbital, on the other hand, finds no ligand combination to interact with, π_0-a_{1g}. The σ diagram is shown in Figure 5.5. The four σ-sp^2 carbon electrons are located at two ligand orbitals: the a_{1g}, completely symmetric and filled, and the e_u, less stable and half filled. The latter ligand orbital makes the triplet the most stable electronic state for the holed D_{4h}-$C_{24}H_{12}$ system. As a result, the four σ-sp^2 electrons (e_u ligand orbital), and not the four π-p_z electrons, determine the electronic state for these holed carbon systems. The main factors affecting the e_u ligand orbital are the distances between the four dangling carbons, the d_x and d_y distances in Figure 5.2a. The triplet is maintained while the d_x and d_y distances are almost identical, but it breaks up to give the singlet when the distances are different. So, the most stable electronic state of D_{4h}-$C_{24}H_{12}$ is a triplet. However, the C_{2v}-C_{58} with the C_{60} geometry is a singlet, d_x = 2.349 Å and d_y = 2.848 Å rather different. In contrast, the C_{2v}-C_{58} with the C_{2v}-$C_{58}Pt$ geometry yields the triplet since d_x and d_y are almost equal: 2.657 Å and

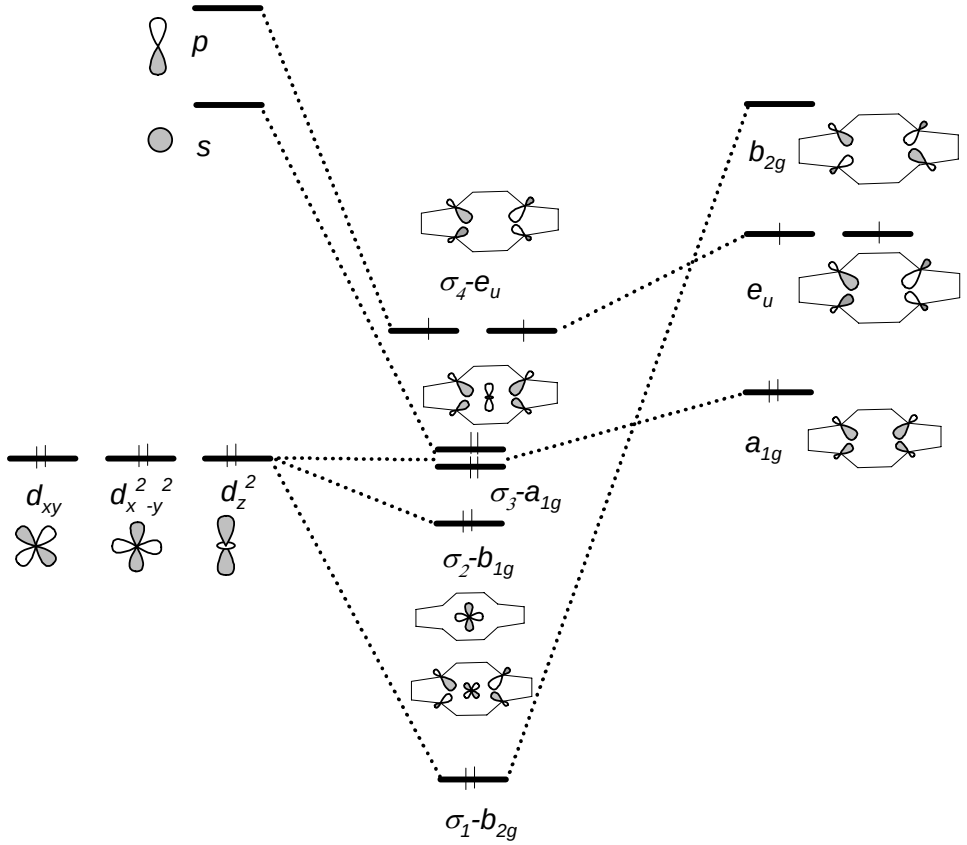

Figure 5.5 Molecular orbital (MO) correlation diagram for σ interaction system between Pt (left, 6 *d* electrons in three metal orbitals) and $C_{24}H_{12}$ (right, 4 sp^2 electrons in three carbon ligand orbitals) for D_{4h}-$C_{26}H_{12}Pt$.

2.665 Å, respectively. Also, the e_u ligand orbital is stabilized by interaction with the empty *p* metal orbitals but it also appears as HOMO (σ_4-e_u) in the MO diagram that gives the triplet as the most stable electronic state of D_{4h}-$C_{24}H_{12}Pt$. The a_{1g} ligand orbital matches the *s* and d_z^2 metal orbitals and gives one of the most bonding interactions: σ_3-a_{1g}. On the other hand, the $d_{x^2-y^2}$ metal orbital is also stabilized by the presence of carbon ligands but it finds no ligand combination to interact with (σ_2-b_{1g}). Finally, the σ_1-b_{2g} is the second most bonding σ MO. It represents the interaction between the d_{xy} metal orbital and the empty σ b_{2g} ligand. To sum up, the triplet is the most stable electronic state of the D_{4h}-$C_{24}H_{12}Pt$ system and the metal-carbon bond

is dominated by (1) two bonding σ MOs: σ_3-a_{1g}, whose carbons transfer a small amount of electron density to metals, and σ_1-b_{2g}, whose metals transfer a considerable amount of electron density to carbon ligands and; (2) two degenerate bonding π MOs included into π_1-e_g. This approximation agrees with the positive net charge on the Pt atom and the negatively charged neighboring carbons in D_{4h}-$C_{24}H_{12}Pt$ and C_{2v}-$C_{58}Pt$.

MOs of C_{2v}-$C_{58}Pt$. The MOs of D_{4h}-$C_{24}H_{12}Pt$ can be easily adapted to the MOs of $C_{58}Pt$ when we take into account two concepts: the curvature of the fullerene surface (C_{4v} symmetry) and the non-equivalency of the four carbons (C_{2v} symmetry). First, we constructed the hypothetical evolution of each MO from the D_{4h}-$C_{24}H_{12}Pt$ system to the C_{2v}-$C_{24}H_{12}Pt$ system, bearing in mind the intermediate curved C_{4v}-$C_{24}H_{12}Pt$ system (Figure 5.6). A posteriori, we demonstrated that the MOs involved in the Pt–C bond for the C_{2v}-$C_{24}H_{12}Pt$ system are a simplification of the MOs found in the C_{2v}-$C_{58}Pt$ heterofullerene. Nevertheless, they provide all the important information for describing the Pt–C bond. The σ and π MOs can mix together when their symmetry changes from D_{4h} to C_{4v}. Basically, this affects the e_u and e_g MOs of the D_{4h} system. After evolution, these MOs become *e* MOs of the C_{4v} system with a high σ-π electron mixing. It is important to remark that the antibonding π_2-e_g MO of the D_{4h} system is transformed to the bonding *6-e* MO of the C_{4v} system due to the considerable presence of σ-sp^2 ligand orbitals. Also, the *7-e* HOMO contains more π-p_z character than its antecessor σ_4-e_u. On the other hand, the σ a_{1g}, b_{1g}, and b_{2g} MOs incorporate p_z contributions to become now a_1, b_1 and b_2 MOs in the C_{4v} system, respectively. In conclusion, the hypothetical C_{4v}-$C_{24}H_{12}Pt$ system would also evolve a triplet as the most stable electronic state. Now, the evolution of the MOs from the C_{4v}-$C_{24}H_{12}Pt$ to the C_{2v}-$C_{24}H_{12}Pt$ will help us to understand the MOs of the $C_{58}Pt$ monoheterofullerene. In this evolution, the equivalency of each carbon is broken and consequently there is a preferred direction for metal-carbon interaction: perpendicular to the orientation of the substituted C_2 unit (d_x direction in Figure 5.2a). The *e* MOs divide into b_2 and b_1 MOs. The most stable MOs are the bonding b_1 MOs with the d_{xz} metal orbital contribution. The d_{xz} metal orbital is perpendicular to the previous C_2 unit. In this orientation, the overlap of the d_{xz} metal orbital with the carbon ligand orbitals is maximum and most effective because the

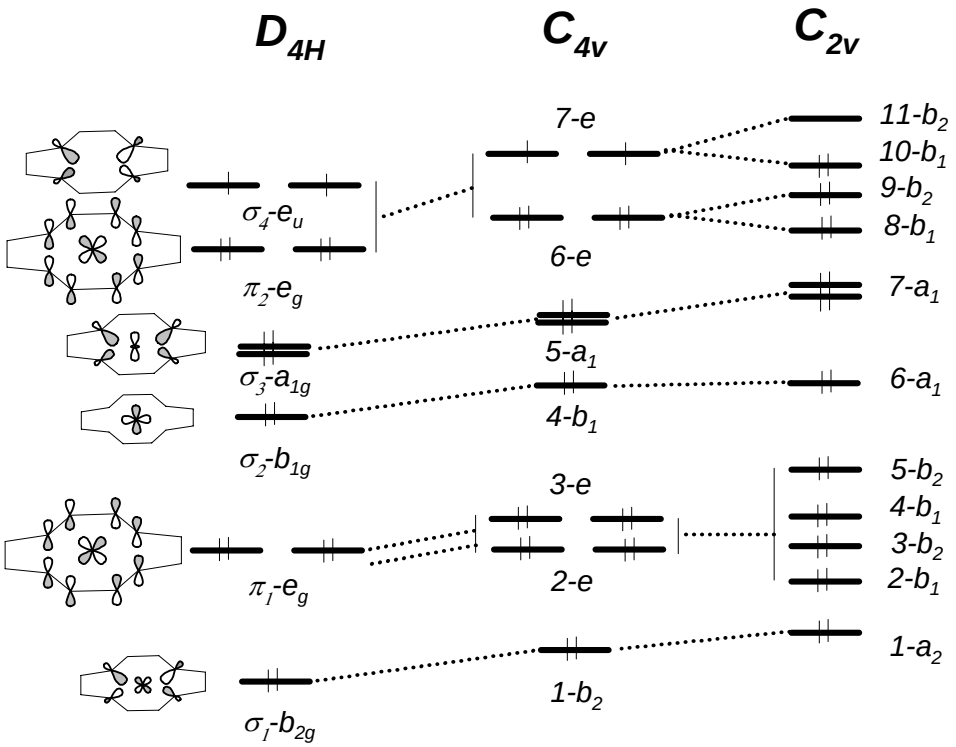

Figure 5.6 Evolution of the molecular orbitals (MOs) of the interaction between a tetracoordinated Pt atom and four carbons with 4 p_z electrons and 4 sp^2 electrons from D_{4h}-$C_{24}H_{12}Pt$ to C_{4v}-$C_{24}H_{12}Pt$ and C_{2v}-$C_{24}H_{12}Pt$. The MOs of the final C_{2v}-$C_{24}H_{12}Pt$ model can be taken as a good simplification of the C_{2v}-$C_{58}M$ MOs.

distances between them are shorter than in the other orientation (compare the d_x with d_y distances in Figure 5.2a for C_{2v} holed heterofullerenes). The analogous d_{yz} metal orbital is represented by the b_2 symmetry in the C_{2v} system. The fact that the stabilization of b_1 MOs is higher than that of b_2 MOs means that the C_{2v}-$C_{58}Pt$ heterofullerene becomes a singlet electronic state with a relatively large HOMO-LUMO gap of 0.59 eV. The triplet state is 0.50 eV above the ground state. Although the *d* metal orbitals are completely spread over several MOs, the contribution of the d_{xz} Pt orbital to *10*-b_1 HOMO is of 21 %, and the contribution of the d_{yz} Pt orbital to *11*-b_2 LUMO is of 13 %. On the other hand, the highly bonding *1*-b_2 MO of the

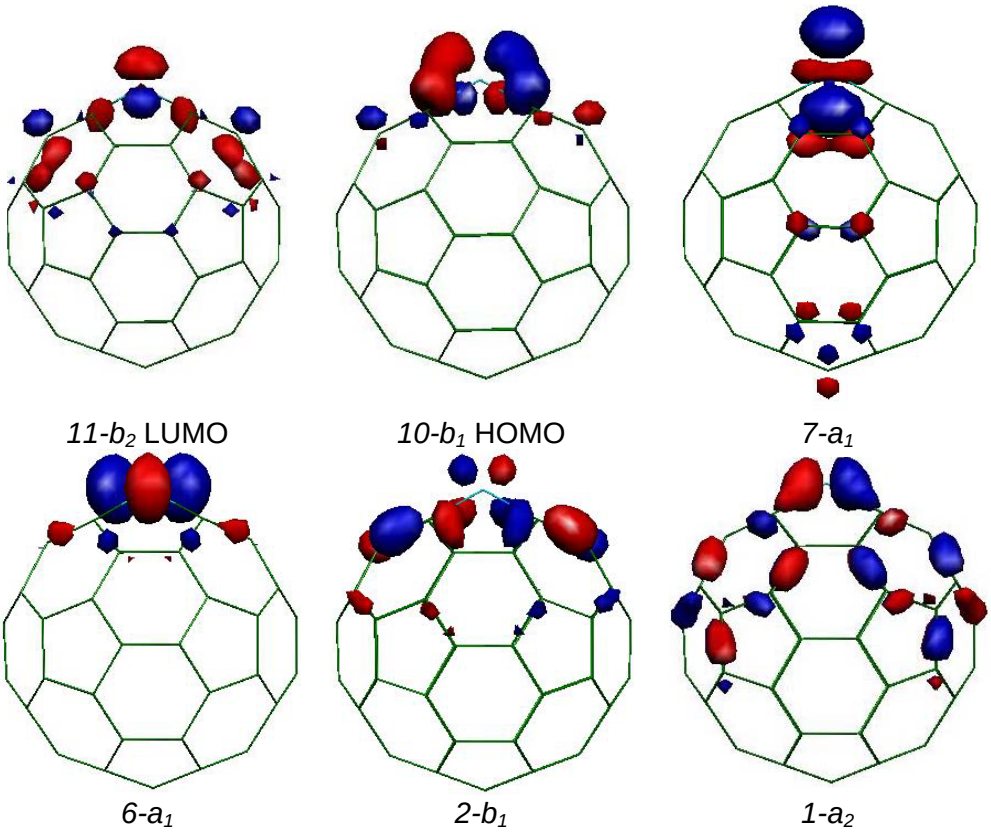

Figure 5.7 The most important molecular orbitals (MOs) of the C_{2v}-C_{58}Pt.

C_{4v} system now becomes the *1-a₂* MO in the C_{2v} system, which retains the σ bonding character of the antecessor. The bonding *5-a₁* MO of the C_{4v} system becomes the *7-a₁* in the C_{2v} system and the stability decreases considerably due to the curvature effect, but it still represents a bonding σ MO. To sum up, the metal-carbon bond in the C_{2v}-C_{58}Pt is basically suspended from: (1) two bonding σ MOs of *1-a₂* and *7-a₁* symmetry between the d_{xy} and d_{z2} metal orbitals and the sp^2 carbon ligand orbitals, respectively; and (2) two bonding π MOs of symmetry b_2 and b_1 between the d_{xz}/d_{yz} metal orbitals and the p_z/sp^2 carbon ligand orbitals spread over several MOs: *2-b₁*, *3-b₂*, *4-b₁*, *5-b₂*, *8-b₁*, *9-b₂* and *10-b₁*. The most important MOs involved in the Pt–C bonds of C_{2v}-C_{58}Pt are plotted in Figure 5.7.

Decomposition of the orbital interaction. The ΔE_{ORB} can be broken up into the contributions made by the orbital interactions within the various irreducible representations of the system's overall symmetry group, in accordance with the decomposition scheme proposed by Ziegler. This decomposition scheme is particularly useful in the complexes considered here because it makes it possible to separate the energy contributions corresponding to σ and π interactions and also to assign these contributions to the corresponding *d* metal orbitals. Table 5.3 shows the results of this energy decomposition for D_{4h}-$C_{24}H_{12}Pt$, C_{2v}-$C_{58}Pt$ and C_s-$C_{58}Pt$. Indeed, the most important contributions that the D_{4h}-$C_{24}H_{12}Pt$ system makes to ΔE_{ORB} are the two σ interactions and the two π interaction: the ligand to metal σ donation through the d_z^2 and the *s* metal orbitals makes a contribution of −19.14 eV (σ_3-a_{1g}), the metal to ligand σ donation through the d_{xy} metal orbital makes a contribution of −8.34 eV (σ_1-b_{2g}) and the two π interactions through d_{xz}/d_{yz} metal orbitals makes a contribution of −4.28 eV (π_1-e_g). As can be seen, σ interactions (−29.56 eV) dominate clearly over π interactions (−7.44 eV) in the insertion of the metal into the planar D_{4h}-$C_{24}H_{12}Pt$ structure. The decomposition of ΔE_{ORB} for C_{2v}-$C_{58}Pt$ shows that σ interactions are reduced dramatically, by almost 9 eV, when the structure is curved from D_{4h}-$C_{24}H_{12}Pt$ to C_{2v}-$C_{58}Pt$. On the other hand, the π interactions even increase by 2.23 eV. This can be attributed to the improvement in the orbital overlap between the d_{xz} metal orbital and the p_z/sp^2 carbon ligand orbitals. The decomposition also shows that the bonding character of d_{xz} (b_1) is stronger than that of d_{yz} (b_2). Subsection 5.2.3 shows that the difference between the C_{2v}-$C_{58}Pt$ and C_s-$C_{58}Pt$ isomers is caused by the energy required for making the hole (ΔE_{HOLE}), but, even so, it is interesting to understand the differences in how the metal is incorporated into both isomers of $C_{58}Pt$. The interaction between C_s-C_{58} and the metal is no different from the interaction of C_{2v}-C_{58} except that two of the four p_z electrons of the dangling bonds in the holed C_s-C_{58} cage are unpaired (Figure 5.2b). The consequence is that the π interactions between the metal and the carbons (*a''* symmetry) increases from −9.67 eV in the C_{2v}-$C_{58}Pt$ to −11.95 eV in the C_s-$C_{58}Pt$. On the other hand the σ interactions (d_{xy}, d_z^2 and *s* represented by *a'* symmetry) are reduced by almost 4 eV in C_s-$C_{58}Pt$, considerably more than in C_{2v}-$C_{58}Pt$. This decrease may be related to the fact that two of the four C−Pt bond lengths increase with respect to the most

Table 5.3 Decomposition of the orbital interaction term (ΔE_{ORB}) for D_{4h}-$C_{24}H_{12}Pt$, C_{2v}-$C_{58}Pt$ and C_s-$C_{58}Pt$ in the irreducible representation of each symmetry [a]

d and p metal orbitals	$C_{24}H_{12}Pt$		$C_{58}Pt$		$C_{58}Pt$	
	D_{4h}		C_{2v}		C_s	
d_z^2, *s*	a_{1g}	–19.14				
$d_{x^2-y^2}$	b_{1g}	–1.89				
--	a_{1u}	0.00				
p_z	a_{2u}	–0.19	a_1	-13.13		
d_{xy}	b_{2g}	–8.34				
--	a_{2g}	0.00	a_2	–7.58	*a'*	–16.87
σ interactions		*–29.56*		*–20.71*		*–16.87*
d_{xz}	e_g	–2.14				
p_x	e_u	–1.58				
--	b_{1u}	0.00	b_1	–6.83		
d_{yz}	e_g	–2.14				
p_y	e_u	–1.58				
--	b_{2u}	0.00	b_2	–2.84	*a''*	–11.75
π interactions		*–7.44*		*–9.67*		*–11.75*
total		*–37.00*		*–30.38*		*–28.62*

[a] Energies in eV.

symmetric isomer (Table 5.1). The sum of both terms accounts for the total ΔE_{ORB}, which is 1.76 eV favorable to the C_{2v}-$C_{58}Pt$ isomer.

5.3 MONOHETEROFULLERENES: $C_{58}M$, $C_{59}M$ (M = Pt, Ir, Os, Ti) and $C_{68}Pt$

5.3.1 $C_{58}M$ (M = Pt, Ir, Os, Ti)

Table 5.4 Geometric properties for C_{2v}-C_{58}M and C_s-C_{58}M (M = Pt, Ir, Os) [a]

$C_{58}M$	*Pt*		*Ir*		*Os*	
Isomer [b]	C_{2v}	C_s	C_{2v}	C_s	C_{2v}	C_s
C–M	2.034	2.049/ 2.013	2.045	2.065/ 1.996	2.058	2.082/ 1.990
Cage radius [c]	3.562	3.569	3.558	3.565	3.556	3.562
HOMA [d]	0.279	0.236	0.308	0.258	0.309	0.274
SE [e]	7.35	7.98	5.43	6.09	5.55	6.12
RE C_s/C_{2v} [f]	–0.63		–0.66		–0.57	

[a] Distances in Å and energy in eV. [b] When Pt replace a C_2 unit in C_{60} two isomer can appear: (1) Pt replaces a 6:6 C_2 bond in the C_{2v} isomer and (2) 6:5 C_2 bond is substituted in the C_s isomer. [c] 3.551 Å for free C_{60}. [d] Harmonic oscillator model of aromaticity (HOMA), 0.274 for free C_{60}. [e] The substitution energy (SE) is defined as the energy reaction of the process $C_{60} + M \rightarrow C_{58}M + C_2$. The true atomic groundstate for M atom is used according to reference: Baerends, E. J.; Branchadell, V.; Sodupe, M. *Chem. Phys. Lett.* **1997**, *265*, 481. [f] Relative energy (RE) between C_s and C_{2v} isomers.

The geometry of both isomers of $C_{58}M$ (M = Pt, Ir, Os, Ti) has been optimized so that effects of substituting different metals in the fullerene carbon framework can be compared. For this purpose, we use the M–C bond lengths, cage radius and also a structure-based measure of aromaticity called the *harmonic oscillator model of aromaticity* (HOMA).[24] HOMA index is probably the most effective index of this kind. The change in aromaticity can also be a measure of how the carbon skeleton of the fullerene is distorted by the irruption of the metal. This relationship is discussed in a recent review of the structural aspects of aromaticity.[25] HOMA varies from 0 for non-aromatic systems to 1 for fully aromatic systems. Table 5.4 shows all the data of the monoheterofullerenes mentioned. Changing the Pt metal for another metal varies the geometric properties only slightly and the structure is rather similar to the structure found for $C_{58}Pt$. The most stable isomer, independently of the metal substitution, is still C_{2v}-$C_{58}M$, which is more stable than the C_s-$C_{58}M$ by *ca.* 0.60 eV. The substitution energy (SE) increases in the order Ir < Os < Ti < Pt. Thus substituting a C_2 unit by M is slightly easier for Ir and Os, around 1.92 and 1.80 eV respectively, than for Pt in the C_{2v}-$C_{58}M$ monoheterofullerenes. The cage radius and the HOMA indexes provide some clues about SE on different metals (Figure 5.8).

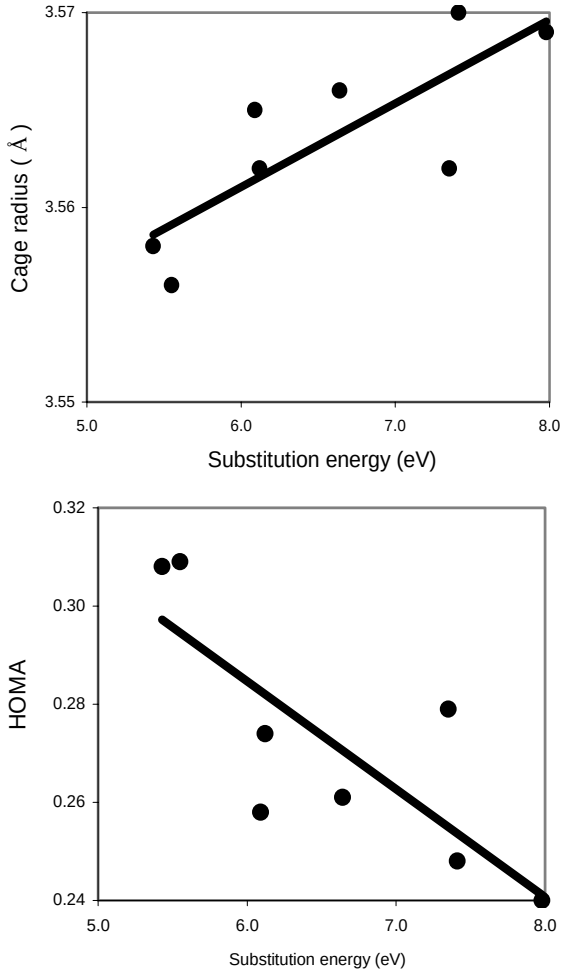

Figure 5.8 Correlation between cage radius and HOMA versus the substitution energy (SE) for C_{2v}-$C_{58}M$ and C_s-$C_{58}M$ (M = Pt, Ir, Os, Ti).

Both geometric parameters are a measure of the cage distortion and it is to be expected that cage distortion and non-aromatic values of HOMA are accompanied by a destabilization of the monoheterofullerenes. Indeed, as can be seen in Figure 5.8, there is a rough correlation between both parameters and SE. So, the most endothermic substitutions found for $C_{58}Pt$ and $C_{58}Ti$ lead to larger cage radius (3.562 and 3.566 Å) and low HOMA values (0.279 and 0.261) whereas $C_{58}Os$ and $C_{58}Ir$, for which the

endothermic substitutions were calculated to be lower, lead to higher HOMA values (0.301 and 0.303) and less cage distortion than C_{60} (lower cage radius: 3.558 and 3.555 Å, respectively). This relationship between geometric parameters and relative stability will be discussed in greater depth with reference to diheterofullerenes (section 5.5).

The SE for $C_{58}M$ (M = Pt, Ir, Os) monoheterofullerenes were decomposed in Table 5.5. This decomposition makes it possible to compare C_s and C_{2v} isomers and also the different metal insertions in the fullerene carbon framework of C_{60}. The energy necessary to make a hole (ΔE_{HOLE}) is the significant energy which determines the most stable isomer: 17.90 eV for C_{2v}-C_{58} and 19.31 eV for C_s-C_{58}. ΔE_{HOLE} is clearly endothermic and favorable to C_{2v}-$C_{58}M$ isomers whereas IBE is exothermic and slightly favorable to C_s-$C_{58}M$ isomers. The geometric parameters (cage radius and HOMA) always suggest that the C_{2v}-$C_{58}M$ isomers will be more stable. C_{2v}-$C_{58}M$ isomers have smaller cage radius and more aromatic HOMA values than C_s-$C_{58}M$ isomers. For instance, the cage radius and HOMA value for C_{2v}-$C_{58}Os$ are computed to be 3.556 Å and 0.309, respectively, and for C_s-$C_{58}Os$, they are 3.562 Å and 0.274. These results can be extrapolated to other pairs of monoheterofullerene isomers. As in $C_{58}Pt$ isomers, the stabilizing IBE values help to form the C_s-$C_{58}M$ isomers but the higher destabilizing ΔE_{HOLE} values help to form the C_{2v}-$C_{58}M$ isomers, which shifts the SE in favour to the latter. This decomposition will be particularly useful to rationalize the decrease in the SE for the series C_{2v}-$C_{58}M$ (M = Pt > Ir ≈ Os) (Pt, 7.35 eV; Os, 5.55 eV and Ir, 5.43 eV). The decrease may be explained by the increase in ΔE_{ORB} from –31.85 eV for Pt to –39.45 eV for Os, which compensates for the expected increase in ΔE_{ST} and ΔE_{DE} due to the larger atomic radii of Os and Ir atoms. It is important to point out that although Ir and Os have larger atomic radii and it could deform the fullerene cage to a much greater extent than Pt atom, they do not do so because these bigger metals protrude a little from the fullerene surface. These atoms still interact with the fullerene carbon framework but do not deform the cage structure. This is reflected by the decrease in the ΔE_{DE} both in the C_{2v}-$C_{58}M$ isomers (1.80 eV for Pt, 1.63 for Ir and 1.71 eV for Os) and the C_s-$C_{58}M$ isomers (1.63 for Pt, 1.53 for Ir and 1. 56 eV for Os) from Pt to Os.

Table 5.5 Decomposition of the substitution energy (SE) for C_{2v}-$C_{58}M$ and C_s-$C_{58}M$ (M = Pt, Ir, Os) [a]

	$C_{58}M$	*Pt*		*Ir*		*Os*	
	Isomer	C_{2v}	C_s	C_{2v}	C_s	C_{2v}	C_s
ΔE_{HOLE} [b]		17.90	19.31	17.90	19.31	17.90	19.31
ΔE_{DE} [c]	C_{58}	1.80	1.63	1.63	1.53	1.71	1.56
	C_2	–0.57	–0.98	–0.57	–0.98	–0.57	–0.98
	M	0.49	0.49	1.36	1.36	2.40	2.40
	Total	1.72	1.14	2.42	1.91	3.54	2.98
ΔE_{INT} [d]	ΔE_{ST}	18.11	16.15	21.99	20.48	22.31	23.13
	ΔE_{ORB}	–30.38	–28.62	–36.88	–35.61	–38.20	–39.30
	Total	–12.27	–12.47	–14.89	–15.13	–15.89	–16.17
IBE [e]		–10.55	–11.33	–12.47	–13.22	–12.35	–13.19
SE		7.35	7.98	5.43	6.09	5.55	6.12
RE C_s/C_{2v} isomers [f]		–0.63		–0.66		–0.57	

[a] Energy in eV. The Substitution Energy (SE) is defined as the energy reaction of the process $C_{60} + M \rightarrow C_{58}M + C_2$ .This energy can be dived into several contributions $SE = \Delta E_{HOLE} + IBE$. [b] ΔE_{HOLE} accounts for the energy reaction of the process $C_{60} \rightarrow C_{58}^* + C_2^*$. Both species C_{58}^* and C_2^* with the fixed geometry of free C_{60}. C_2* keeps the electronic configuration as its free C_2 analogue whereas C_{58}^* is calculated at the most stable electronic state in this geometry, a singlet. [c] ΔE_{DE} accounts for the deformation energy for the three fragments: $C_{58}^* \rightarrow C_{58}$, $C_2^* \rightarrow C_2$ and $M \rightarrow M^*$. C_{58} with the fixed geometry found in $C_{58}M$ and a triplet as the most stable electronic state. C_2 geometrical optimised. M is calculated at the most stable electronic state (unrestricted) and M* at restricted electronic state. [d] ΔE_{INT} accounts for the interaction energy between the C_{58} and M* fragments at the fixed $C_{58}M$ geometry. [e] IBE (insertion binding energy) accounts for the energy reaction of the process $C_{58}^* + C_2^* + M^* \rightarrow C_{58}M + C_2$. Also, $IBE = \Delta E_{DE} + \Delta E_{INT}$. [f] Relative energies (RE) between C_{2v} and C_s isomers.

5.3.2 $C_{68}Pt$, a doped fullerene from D_{5h}-C_{70}.

Finally, to find out more about the relationship between the substituted C–C bond and its stabilization, we constructed all possible hypothetical regioisomers by replacing a C_2 unit with a Pt atom in the C_{70}

Table 5.6 Characterization of the eight distinct regioisomers of $C_{68}Pt$, a doped fullerene from the free D_{5h}-C_{70}:**1** [a]

Isom.	*Sym.*	*C–C bond type* [b]	*C–C bond lenghts*	θ_p [c]	*MBO* [d]	*Cage Radius* [e]	*HOMA* [f]	*RE* [g]
d,e	C_1	***B***	1.421	9.43	1.246	3.855	0.337	0.00
c,c	C_s	pyracylene, ***A***	1.393	11.49	1.332	3.847	0.353	0.01
a,b	C_s	pyracylene, ***A***	1.399	11.92	1.334	3.842	0.350	0.06
c,d	C_1	corannulene, ***D***	1.446	10.88	1.138	3.855	0.318	0.63
b,c	C_1	corannulene, ***D***	1.448	11.73	1.140	3.851	0.323	0.69
a,a	C_s	corannulene, ***D***	1.451	11.85	1.138	3.848	0.321	0.83
e,e	C_{2v}	pyrene, ***C***	1.470	8.60	1.167	3.861	0.300	0.93
d,d	C_s	corannulene, ***D***	1.438	10.28	1.219	3.859	0.327	1.19

[a] Distances in Å, angles in º and energy in eV. [b] The different C–C bond types in the IPR fullerenes can be visualized in Appendix A.1 [c] Pyramidalization angle (θ_p). [d] Mayer bond order (MBO). [e] Cage Radius is defined as the average distance of all surface atoms to the center of the fullerene. Cage radius for D_{5h}-C_{70} is 3.837 Å. [f] The HOMA index for D_{5h}-C_{70}:1, 0.362. [g] Relative energies (RE).

fullerene. Basically, the C–C bonds are characterized by their different pyramidalization angles (θ_p), distances and topologies. The C_{70} fullerene is highly suitable because it contains eight different C–C bonds with different pyramidalization angles unlike the previous C_{60} studied. Only one isomer obeys the isolated pentagon rule (IPR) for the C_{70} stoichiometry.[26] This structure, which is of D_{5h} symmetry, has five types of carbons, which form nine layers. These carbons are connected by eight different C–C bond types, four of which occur at 6:6 ring junctions: Ca–Cb, Cc–Cc, Ce–Ce and Cd–Ce. The first two are pyracylene types while the third is a pyrene type (see Appendix A.4 for a full description of the distinct C–C bonds). The C_{70} is most curved at the poles and flatter at the equator. The flat area in the middle is the most aromatic and has a low Mayer bond order (MBO) whereas in the more curved area the C–C bonds have a greater double bond character and higher MBOs. Table 5.6 shows the characterization of all eight distinct C–C bonds and the relative energies (RE) of the eight $C_{68}Pt$ regioisomers.

Three regioisomers corresponding to the 6:6 Ca–Cb, Cc–Cc and Cd–Ce substitutions appear very close in energy (0.00-0.06 eV) and are the most stable regioisomers. The other regioisomers are much less stable (by 0.63-1.19 eV). The Ca–Cb and Cc–Cc structures represent doping at the poles whereas the Cd–Ce represents doping in the flat area. This last regioisomer was not expected to be as stable as it is found. Apart of this discrepancy, some conclusions can be drawn from the data in Table 5.6. First, the substitution of a 6:6 C–C bond seems to be particulary important, except when the pyramidalization angle and MBO of the bond are extremely low: for example the Ce–Ce bond. Second, the MBO is a good reference for the double bond localization and the substitution in these sites is favoured. The three most stable regioisomers are those in which the three C–C bonds with the highest MBOs have been substituted. Third, the pyramidalization angle seems not to have a crucial effect on the stabilization and shows unambiguous results. We would need more data on other heterofullerenes to draw any conclusions about the effect of the pyramidalization angle on the substitution patterns. Finally, the fourth conclusion is maybe the most important: the regioisomer constructed with the smallest change in the aromaticity will become the most stable regioisomer. The three most stable regioisomers have the three highest aromatic HOMA values: 0.337, 0.353 and 0.350. This was also observed in the section above for the $C_{58}M$ monoheterofullerenes constructed from the C_{60}. On the other hand, the SE was computed to be 7.50 eV for the most stable $C_{68}Pt$ isomer which is rather similar to the SE for C_{2v}-$C_{58}Pt$, 7.35 eV.

5.3.3 $C_{59}M$ (M = Pt, Ir, Os, Ti)

The substitution of one carbon by one metal results in the formation of the $C_{59}M$ heterofullerenes. This tricoordinated metal protrudes from the fullerene surface because there is no space for it to be included completely, unlike the $C_{58}M$ heterofullerenes. The geometrical parameters for $C_{59}M$ (M = Pt, Ir, Os, Ti) are listed in Table 5.7 and an optimized geometry of $C_{59}Pt$ is displayed in Figure 5.1. The Pt–C bond lengths in the $C_{59}M$ heterofullerene are somewhat shorter than in their homologous $C_{58}M$ heterofullerene. For example, the mean Pt–C bond length in $C_{59}Pt$ is 1.961 Å and in C_{2v}-$C_{58}Pt$ it is 2.016 Å. The electronic configuration of $C_{59}Pt$ is a singlet closed-shell in

Table 5.7 Geometric properties for $C_{59}M$ (M = Pt, Ir, Os, Ti) [a]

	$C_{59}Pt$	*$C_{59}Ir$*	*$C_{59}Os$*	*$C_{59}Ti$*
M–C [b]	1.998/ 1.951	1.962/ 1.921	1.951/ 1.892	2.020/ 1.939
Cage radius [c]	3.580	3.578	3.578	3.581
Substitution energy (SE) [d]	6.20	3.51	3.46	4.69

[a] Distances in Å and energy in eV. [b] The longest M–C bond lengths occur between the metal and the carbons which belong to a hexagon while the shortest ones occurs between the metal and the carbon atom which belong to the pentagon. [c] 3.551 Å for C_{60}, 3.562 Å, 3.558 Å and 3.556 Å for C_{2v}-$C_{58}M$ (M = Pt, Ir Os), respectively. [d] The Substitution energy (SE) is defined as the energy reaction of the process $C_{60} + M \rightarrow C_{59}M + C$. The true atomic groundstate for M and C atom is used according to reference: Baerends, E. J.; Branchadell, V.; Sodupe, M. *Chem. Phys. Lett.* **1997**, *265*, 481.

which the HOMO-LUMO gap was computed to be 0.70 eV. The triplet structure with one electron in the HOMO and another in the LUMO was also optimized but its relative energy with respect to the singlet structure was quite high (0.44 eV). Mulliken population analysis indicates that there is significant electron charge transfer from the metal to the carbon fragment. The net charge on platinum is +0.76 *e*. The electronic populations of the *s*, *p* and *d* Pt orbitals are 2.547, 6.313 and 8.385 *e*, respectively. The metal orbitals in $C_{59}Pt$ are spread over a wide range of MOs. Each of these MOs in the metallofullerene has a low metal contribution. Specifically, the participation of the metal orbitals is 17% in the HOMO and 20% in the LUMO. The ground state for the analogue iridium cluster is a doublet in which the spin density is quite delocalized with 0.21 *e* on the metal center, 0.29 *e* on the nearest carbon and the rest of the spin density delocalized through the carbon cage in smaller increments. Mulliken population analyses suggest that the electron charge transfer from the metal to the fullerene is somewhat lower than in the platinum analogue.

The substitution of one carbon by one metal does not lead to the same cage deformation as in $C_{58}M$ monoheterofullerenes. In consequence, the SE is reduced considerably more in $C_{59}M$ than in $C_{58}M$. Indeed, for Ir and Os, the SE was computed to be less endothermic when a C atom is substituted rather than a C_2 unit. In this stoichiometry no correlation between the SE, the cage radius and HOMA values is appreciated (compare values in Table 5.7). Table 5.8 shows the decomposition of SE for $C_{59}M$ heterofullerenes. The SE value in this stoichiometry is lower because: (1) the energy required to make the tricoordinated holed C_s-C_{59} fullerene is

Table 5.8 Decomposition of the substitution energy (SE) for $C_{59}M$ (M = Pt, Ir, Os) [a]

		$C_{59}M$ Isomer	Pt C_s	Ir C_s	Os C_s
ΔE_{HOLE} [b]			16.85	16.85	16.85
IBE [c]	ΔE_{DE} [d]	C_{59}	–0.47	–0.19	0.01
		C	–1.27	–1.27	–1.27
		M	0.49	1.36	2.40
		Total	–1.25	–0.10	1.14
	ΔE_{INT} [e]	ΔE_{ST}	14.78	20.30	24.22
		ΔE_{ORB}	–24.18	–33.54	–38.75
		Total	–9.40	–13.24	–14.53
	Total		–10.65	–13.34	–13.39
SE [a]			6.20	3.51	3.46

[a] Energy in eV. The SE is defined as the energy reaction of the process $C_{60} + M \rightarrow C_{59}M + C$. This energy can be dived into several contributions, $SE = \Delta E_{HOLE} + IBE$. [b] ΔE_{HOLE} accounts for the energy reaction of the process $C_{60} \rightarrow C_{59}^* + C^*$. C_{59}^* with the fixed geometry of free C_{60} and triplet as the most stable electronic state. [c] IBE (insertion binding energy) accounts for the energy reaction of the process $C_{59}^* + C^* + M^* \rightarrow C_{59}M + C$. $IBE = \Delta E_{DE} + \Delta E_{INT}$. [d] ΔE_{DE} accounts for the deformation energy for the three fragments: $C_{59}^* \rightarrow C_{58}$, $C^* \rightarrow C$ and $M \rightarrow M^*$. C_{59} with the fixed geometry found in $C_{59}M$ and a singlet as the most stable electronic state. C and M are calculated at the most stable electronic state (unrestricted) and C* and M* always at restricted electronic state. [e] Finally, ΔE_{INT} accounts for the interaction energy between the fragments C_{59} and M* at the fixed $C_{59}M$ geometry.

substantially lower (ΔE_{HOLE} = 16.85 eV, which is 1.05 eV lower than the energy required to create a holed C_{2v}-C_{58} fullerene) and (2) no deformation energy (ΔE_{DE}) is required to adapt the C_s-C_{59} geometry of C_{60} to the C_s-C_{59} geometry in $C_{59}M$. On the other hand, ΔE_{INT} is less favorable in the tricoordinated Pt than in the tetracoordinated Pt because the overlap between the metal orbitals and the carbon ligand orbitals is less effective. The SE for $C_{59}M$ also follows the same trend for the different metals as $C_{58}M$ does. $C_{59}M$ heterofullerenes (M = Os, Ir) are easier to construct than the $C_{59}Pt$ homologues: 6.20 eV for $C_{59}Pt$, 3.51 eV for $C_{59}Ir$ and 3.46 eV for $C_{59}Os$ are the values for the SE.

Table 5.9 Substitution energy (SE) for cation, neutral and anion C_xM (x = 58, 59; M = Pt, Ir, Os) clusters [a]

Heterofullerene	*M*	*cation*	*neutral*	*anion*
$C_{58}M$ [b]	*Pt*	7.16	7.35	6.57
	Ir	4.94	5.43	4.81
	Os	5.41	5.55	5.08
$C_{59}M$ [c]	*Pt*	5.32	6.20	6.03
	Ir	2.37	3.51	3.27
	Os	2.90	3.46	3.39

[a] Energies in eV. [b] The SE for $C_{58}M$ is defined as the energy reaction of the process $C_{60} + M \rightarrow C_{58}M + C_2$. [c] For $C_{59}M$ is defined as the energy reaction of the process $C_{60} + M \rightarrow C_{59}M + C$. The true atomic groundstate for M and C atoms is used according to reference: Baerends, E. J.; Branchadell, V.; Sodupe, M. *Chem. Phys. Lett.* **1997**, *265*, 481.

5.3.4 Stability of neutral monoheterofullerenes versus cation and anion analogues

At the present level of theory, the BE per atom for C_{60} is 7.36 eV. In general, the C substitution by a metal in the free C_{60} is a highly endothermic process. The SE of a C atom by a Pt atom in C_{60} is computed to be 6.20 eV and the BE per atom for $C_{59}Pt$ is reduced to 7.25 eV. When the metal replaces a 6:6 C_2 bond to give $C_{58}Pt + C_2$, the SE involved is 7.35 eV and the BE per atom is equal to that of the $C_{59}Pt$, 7.25 eV. However, we are also interested in the cation and anion because these monoheterofullerenes are detected via positive or negative ion mode in the mass spectrum studies. The oxidation or reduction of these neutral monoheterofullerenes may seriously affect their stability. The SEs for the cationic, neutral and anionic monoheterofullerenes of $C_{58}M$ and $C_{59}M$ (M = Pt, Ir, Os) are listed in Table 5.9. Independently of the metal, all cations and anions are easier to obtain than their respective neutral monoheterofullerene. The SE is reduced for all cases. Nevertheless, each monoheterofullerene has a different stabilization pattern: $C_{58}M$ follows the trend: anion > cation > neutral while $C_{59}M$ follows the trend: cation > anion > neutral. So the easiest way to obtain $C_{58}M$ and $C_{59}M$ monoheterofullerenes will be in the negative ion mode and the positive ion modes, respectively.

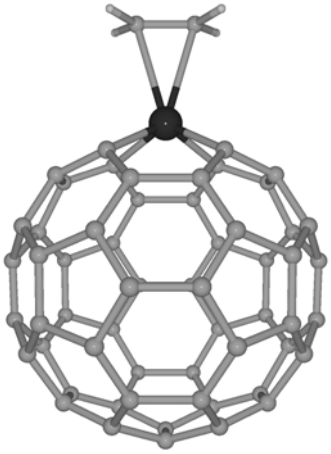

Figure 5.9 Optimized structure for $[C_{58}Ir(C_2H_4)]^-$.

5.4 ADDITION OF ETHYLENE TO MONOHETEROFULLERENES

5.4.1 Experimental evidence

In order to demonstrate that the metals in these newly formed clusters were indeed on the outside of the fullerene, they were exposed to added substrates. Experimentalists have investigated the reactions of these new cluster ions with a potential ligand, 2-butene. The high mass portion of the spectrum acquired upon laser ablation of a $C_{60}/Ir(CO)_2$ film in an atmosphere of 2-butene reveals several new species including: $[C_{59}Ir(2\text{-butene})]^-$, $[C_{58}Ir(2\text{-butene})]^-$, $[C_{57}Ir(2\text{-butene})]^-$ and $[C_{56}Ir(2\text{-butene})]^-$. Clearly, the metal ions in $C_{60-x}Ir^-$ with both x odd and x even can add an external ligand. Similar experiment were carried out with laser ablation of a C_{60}/Pt film in the presence of 2-butene. In this case only one new species, $[C_{57}Pt_2(2\text{-butene})]^-$, was revealed. The ions $C_{58}Pt^-$, $C_{56}Pt^-$, $C_{58}PtO^-$ and $C_{56}PtO^-$ appeared to be unreactive toward the bonding of 2-butene. It is particularly interesting to note that both $C_{58}Ir^-$ and $C_{56}Ir^-$ bind 2-butene while $C_{58}Pt^-$ and $C_{56}Pt^-$ are unreactive under similar conditions. In view of the low reactivity of $C_{58}Pt^-$ and $C_{56}Pt^-$ toward 2-butene, the reactivity of

Table 5.10 Geometric and electronic properties for cation, neutral and anion $C_{58}Ir(C_2H_4)$ and $C_{58}Pt(C_2H_4)$ complexes [a]

Mole.		$[C_{58}M(C_2H_4)]^+$	$C_{58}M(C_2H_4)$	$[C_{58}M(C_2H_4)]^-$
Ir	*M–C (fullerene)* [a]	2.036	2.039	2.038
	M–C	2.749	2.479	2.236
	C–C (ethylene) [b]	1.352	1.373	1.425
	Cage Radius [c]	3.556	3.556	3.559
	Transfer cage $\rightarrow C_2H_4$	–0.316	–0.196	0.138
Pt	*M–C (fullerene)* [d]	2.005	2.009	2.012
	M–C	2.447	2.447	2.435
	C–C (ethylene)	1.371	1.373	1.375
	Cage Radius [e]	3.556	3.557	3.560
	Transfer cage $\rightarrow C_2H_4$	–0.258	–0.166	–0.062

[a] Values in Å. [b] M–C bond lengths for $C_{58}Ir^+$, $C_{58}Ir$ and $C_{58}Ir^-$ are 2.037 Å, 2.033 Å and 2.039 Å, respectively. [b] The C–C distance in the free C_2H_4 molecule is 1.333 Å. [c] The cage radius for $C_{58}Ir^+$, $C_{58}Ir$ and $C_{58}Ir^-$ are 3.554 Å, 3.558 Å and 3.561 Å, respectively. [d] M–C bond lengths for $C_{58}Pt^+$, $C_{58}Pt$ and $C_{58}Pt^-$ are 2.025 Å, 2.016 Å and 2.018 Å, respectively. [e] The cage radius for $C_{58}Pt^+$, $C_{58}Pt$ and $C_{58}Pt^-$ are 3.558 Å, 3.561 Å and 3.564 Å, respectively.

$C_{59}Pt^+$ toward addition was also examined. $C_{59}Pt^+$ adds 2-butene to form $[C_{59}Pt(2\text{-butene})]^+$. Calculations were carried out to analyze the reactivity of cationic, neutral and anionic $C_{58}M$ (M = Pt, Ir) structures with ethylene as a model for 2-butene.

5.4.2 Interaction between ethylene and monoheterofullerenes

Calculations were also carried out to analyze the reactivity of $C_{58}M^-$, $C_{58}M$ and $C_{58}M^+$ (M = Pt, Ir) with 2-butene. To simplify the problem and to save computer time, the 2-butene ligand was modeled as an ethylene molecule. The computed structure of $[C_{58}Ir(C_2H_4)]^-$ is shown in Figure 5.9. The ethylene ligand coordinates to the metal in the C_{2v}-$C_{58}M$ clusters without altering the structure of the fullerene as the values in Table 5.10

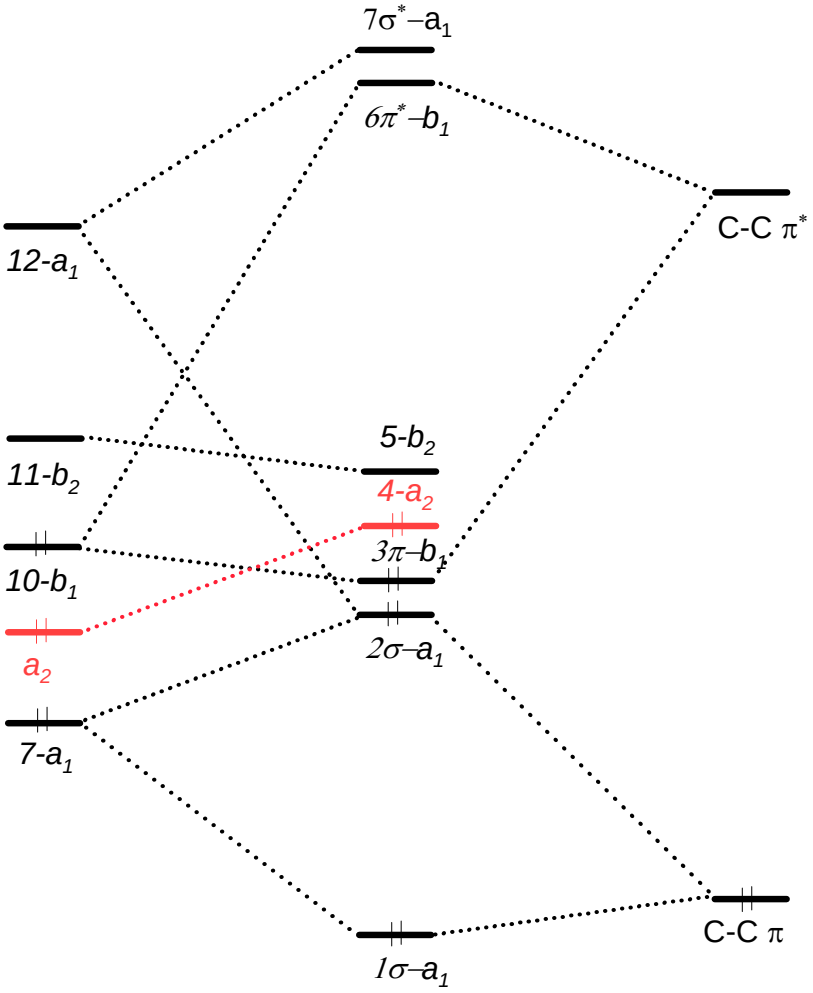

Figure 5.10 Molecular orbital (MO) correlation diagram for the interaction between C_2H_4 ligand (right) and $C_{58}Ir^-$ (left) in order to construct the $[C_{58}Ir(C_2H_4)]^-$ complex (only black lines). The addition of the red lines converts the draw to the MO correlation diagram of $C_{58}Pt(C_2H_4)$ cluster.

show. All the structures were optimized under the C_{2v} symmetry constraints. The process:

(5.3) $C_{58}M + C_2H_4 \rightarrow C_{58}M(C_2H_4)$ (M = Pt or Ir)

is exothermic for neutral, monoanionic and monocationic molecules. The formation energy of $[C_{58}Ir(C_2H_4)]^-$ from $C_{58}M^-$ and C_2H_4 units was computed to be 0.68 eV. This relatively large value is consistent with the experimental observation of a peak in the mass spectrum that may be associated to $[C_{58}Ir(2\text{-butene})]^-$. It is also consistent with a metal-ligand distance of 2.236 Å, which is only somewhat longer than in conventional organometallic iridium complexes, in which the Ir–C bond lengths range between 2.03 and 2.21Å.[27] The energy involved in the formation of the analogous complex of platinum, $[C_{58}Pt(C_2H_4)]^-$, is –0.54 eV. Although $[C_{58}Pt(2\text{-butene})]^-$ was not observed in the laser ablation experiment using a C_{60}/Pt film in the presence of 2-butene, current DFT calculations do not exclude that the $C_{58}Pt^-$ fullerene may coordinate the double C–C bonds through the platinum atom. We also included the neutral and monocationic species in our study because the comparison can be quite useful for understanding the bonding features between both fragments.

The correlation diagram of $[C_{58}Ir(C_2H_4)]^-$ in Figure 5.10 shows the origin of the σ donation and π back-donation interactions between the frontier MOs of C_{2v}-$C_{58}Ir^-$ and those of the C_2H_4 fragment. The MO of C_{2v}-$C_{58}Ir^-$ is a slight variation on the MO of C_{2v}-$C_{58}Pt$ in Figure 5.7 because both molecules are isoelectronic. The σ donation to the empty metal orbitals involves the occupied orbital in C_2H_4 with C–C π character and two metal orbitals of the monoheterofullerene with d_{z2} + *s* character: *7*-a_1 and *12*-a_1. The resulting MOs are two bonding occupied σ MOs (*1*σ-a_1 and *2*σ-a_1) and one highly destabilized unoccupied MO (*7*σ^*-*a1*). The π back-donation mainly involves the C_{2v}-$C_{58}Ir^-$ HOMO (*10*-b_1) and the π^*_{C-C} LUMO of the C_2H_4 ligand. Now, the resulting MOs are the HOMO of the interacted system (*3*π-b_1) and another highly destabilized orbital (*6*π^*-b_1). The LUMO of the final adduct (*5*-b_2) is almost the LUMO of the C_{2v}-$C_{58}Ir^-$ monoheterofullerene (*11*-b_2). The correlation diagram for isoelectronic $C_{58}Pt(C_2H_4)$ differs from this model only in the HOMO designation. The interaction destabilizes the a_2 orbitals and one of them becomes the HOMO of the final adduct (*4*-a_2), thus replacing the π back-donation (*3*π-b_1) in this function. The diagram for the analogue complexes $[C_{58}Ir(C_2H_4)]^+$, $C_{58}Ir(C_2H_4)$, $[C_{58}Pt(C_2H_4)]^+$ and $[C_{58}Pt(C_2H_4)]^-$ is easily constructed by

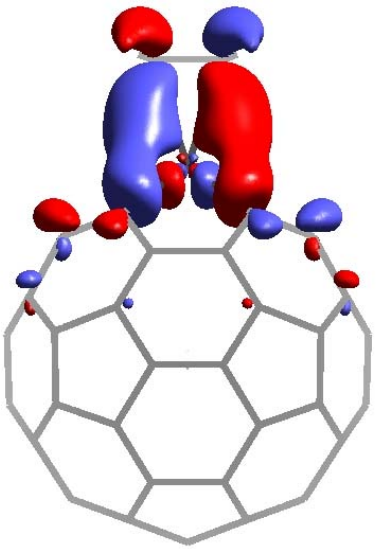

Figure 5.11 3D representation of the HOMO of $[C_{58}Ir(C_2H_4)]^-$, 3π-b_1 in Figure 5.10. The π back-donation orbital from *d* Ir filled orbitals to the empty π *C–C ethylene orbital.

removing or adding electrons from the above mentioned well-known diagrams of $C_{58}Pt(C_2H_4)$ and $[C_{58}Ir(C_2H_4)]^-$.

To characterize the heterofullerene-ethylene bond we used an extension of the Morokuma decomposition scheme developed by Ziegler and Rauk to decompose the BE. According to this scheme, the BE between the fullerene and the ethylene can be decomposed into three main contributions: ΔE_{DE}, ΔE_{ST} and ΔE_{ORB}. More details about this decomposition can be found in subsection 4.2.4. The various terms of the BE partition for the cationic, neutral and anionic complexes $C_{58}M(C_2H_4)$ (M = Ir, Pt) are given in Table 5.11 and Table 5.12. For $C_{58}Ir(C_2H_4)$, the deformation energy (ΔE_{DE}) is only 0.19 eV because the deformation of both cage and ethylene units with respect to the isolated molecules is very small. The Pauli repulsion, 4.76 eV, is larger than the electrostatic term, –3.20 eV, and, therefore, the steric term (ΔE_{ST}) that is the sum of these two contributions is repulsive: +1.56 eV. The orbital term (ΔE_{ORB}), which is –2.16 eV, overcomes the ΔE_{ST} and the ΔE_{DE} of the fragments and is responsible for the adduct formation. The examination of the ΔE_{ORB} values

Table 5.11 Decomposition of the binding energy (BE) for $C_{58}Ir(C_2H_4)$ [a]

		$[C_{58}Ir(C_2H_4)]^+$	$C_{58}Ir(C_2H_4)$	$[C_{58}Ir(C_2H_4)]^-$
ΔE_{DE}	*Cage*	0.04	0.12	0.25
	Ethylene	0.02	0.07	0.40
	Total	0.06	0.19	0.65
ΔE_{ST}	ΔE_{Pauli}	2.06	4.76	9.84
	ΔE_{elstat}	–1.45	–3.20	–6.66
	Total	0.61	1.56	3.18
ΔE_{ORB}	$\Delta E_{a1}(\sigma)$	–0.93	–1.32	–1.96
	ΔE_{a2}	–0.02	–0.03	–0.04
	$\Delta E_{b1}(\pi)$	–0.11	–0.71	–2.32
	ΔE_{b2}	–0.07	–0.10	–0.19
	Total	–1.13	–2.16	–4.51
ΔE_{INT}		–0.52	–0.60	–1.33
BE [b]		–0.46	–0.41	–0.68

[a] Values in eV. [b] The BE is the energy difference between the optimized $C_{58}Ir(C_2H_4)$ adduct and the two relaxed $C_{58}Ir$ and C_2H_4 fragments.

exemplify that the interactions of the a_1 symmetry, which give the σ donation from the π ethylene orbital to the metal orbitals, clearly make the largest contribution to ΔE_{ORB}, –1.32 eV. The contribution associated to the b_1 symmetry, which accounts for the π back-donation, is approximately half this value (–0.71 eV). The other symmetries are almost negligible. In contrast, when the fullerene acts as a ligand in complexes such as (η^2-C_{60})$M(PH_3)_2$ (M = Ni, Pd, Pt), Sgamelloti and co-workers have demonstrated that the π back-donation from the metal to the fullerene is more important than the corresponding ligand to metal σ donation.[28] This idea will be discussed at length in Chapter 6.

The addition of one electron to the single occupied bonding MO of 3π-b_1 symmetry in $C_{58}Ir(C_2H_4)$ shortens the M–ethylene bond lengths from 2.479 Å in the neutral complex to 2.236 Å in the reduced complex. This

shortening is accompanied by a larger deformation of the ethylene fragment, the ΔE_{DE} term increasing to 0.65 eV. The repulsive ΔE_{ST} and ΔE_{ORB} terms also increase after reduction and the total Ir–ethylene BE is greater by 0.27 eV when the π back-donation orbital represented in Figure 5.11 accommodates two electrons. The values in Table 5.11 show that in the anionic $[C_{58}Ir(C_2H_4)]^-$ complex the contribution of b_1 MOs to the ΔE_{ORB} term is larger that of the electron density rearrangement associated with the mixing between a_1 MOs, which suggests that in $[C_{58}Ir(C_2H_4)]^-$ the π back-donation is more important than the σ donation. In the other case, when the only electron of the bonding 3π-b_1 HOMO is removed, the M-ethylene distance lengthen considerably to 2.749 Å in the oxidized complex. However, the lower interaction of both fragments does not drastically reduce BE. This is because ΔE_{INT} is reduced drastically, as expected, from –2.16 eV in the neutral complex to –1.13 eV in the oxidized complex, but the ΔE_{DE} and ΔE_{ST} are also reduced. The final BE is 0.05 eV more stable than in the neutral complex. There is an association between the lower interaction between the two fragments and the shorter C–C distance in the ethylene of the oxidized complex. (1.352 Å, 1.373 Å and 1.425 Å in the $[C_{58}Ir(C_2H_4)]^+$, $[C_{58}Ir(C_2H_4)]$ and $[C_{58}Ir(C_2H_4)]^-$, respectively).

As expected from the isoelectronic nature of $C_{58}Pt(C_2H_4)$ and $[C_{58}Ir(C_2H_4)]^-$, these two complexes have similar BEs (Table 5.11 and Table 5.12). However, in the platinum complex the coordination distance between the ethylene and the transition metal is quite long (2.447 Å). This value is similar to the computed value for the neutral iridium complex. Usually, the Pt(0)–ethylene bond length is close to 2.10 Å,[29] and many theoretical studies have shown that the Pt(0)–ethylene bond in (η^2-CH_2=CH_2)$Pt(PH_3)_2$ is stronger, with dissociation energies (DEs) between 0.87 and 1.21 eV.[30] Therefore one can conclude from present studies that π ligands might coordinate to $C_{58}Pt$ but with an interaction that is weaker than that in the diphenylphosphine complexes. The partitioning energy values for $C_{58}Pt(C_2H_4)$ indicate that the orbital term is clearly dominated by the σ donation, as it is in the neutral Ir-complex. In other words, the ligand→metal σ donation is more effective than the metal→ligand π back-donation at long M–ethylene bond lengths. For an extensive discussion on

Table 5.12 Decomposition of the binding energy (BE) for $C_{58}Pt(C_2H_4)$ [a]

		$[C_{58}Pt(C_2H_4)]^+$	$C_{58}Pt(C_2H_4)$	$[C_{58}Pt(C_2H_4)]^-$
ΔE_{DE}	*Cage*	0.22	0.12	0.16
	Ethylene	0.07	0.07	0.08
	Total	0.29	0.19	0.24
ΔE_{ST}	ΔE_{Pauli}	4.63	4.72	5.17
	ΔE_{elstat}	–3.09	–3.20	–3.43
	Total	1.54	1.52	1.74
ΔE_{ORB}	$\Delta E_{a1}(\sigma)$	–1.73	–1.58	–1.50
	ΔE_{a2}	8.94	–0.02	–0.02
	$\Delta E_{b1}(\pi)$	–9.73	–0.73	–0.88
	ΔE_{b2}	–0.10	–0.09	–0.12
	Total	–2.62	–2.42	–2.52
ΔE_{INT}		–1.08	–0.90	–0.78
BE [b]		–0.79	–0.71	–0.54

[a] Values in eV. [b] The BE is the energy difference between the optimized $C_{58}Pt(C_2H_4)$ adduct and the two relaxed $C_{58}Pt$ and C_2H_4 fragments.

the nature of the bonding in transition metal complexes see the recent review by Frenking and Frölich.[31]

The reduction of the neutral platinum complex to give $[C_{58}Pt(C_2H_4)]^-$ differs from the iridium complex because the added electron goes to a non-bonding MO of b_2 symmetry (*5*-b_2) between the heterofullerene and the ethylene ligand. Consequently, the orbital interaction and the deformation energy of both fragments are not modified significantly. The C–C bond in ethylene remains almost invariant whereas the Pt–ethylene bond increases only slightly (0.012 Å). The smaller BE for the anionic $[C_{58}Pt(C_2H_4)]^-$ cluster can be attributed to an increase in the Pauli repulsion between the ethylene and the negatively charged heterofullerenes, from 4.72 eV in the neutral complex to 5.17 eV in the reduced system. In no way does the oxidation change the geometry of the

$C_{58}Pt(C_2H_4)$ cluster. However, the removal of one electron of *4-a_2* symmetry containing only cage electrons significantly changes the contribution of each irreducible representation of the ΔE_{ORB} term. In conclusion, the BE is favored a little in the oxidation process and the addition of ethylene to $C_{58}Pt^+$ has a value that is 0.08 eV more favorable than the neutral complex.

It is important to mention the inverse order of BE for the interaction of $C_{58}M$ and C_2H_4 fragments in the cationic, neutral and anionic mode of the monoheterofullerene species. For the iridium atom the most favorable interaction will appear between the anionic species whereas for the platinum atom it will appear between the cationic species.

5.5 DIHETEROFULLERENES: $C_{57}Pt_2$, $C_{56}Pt_2$ and $C_{81}Pt_2$

A systematic search of the regioisomers of the heterofullerenes, $C_{57}Pt_2$ and $C_{56}Pt_2$, was made through density functional calculations in order to find the most stable structures. Both heterofullerenes incorporate two metals into the fullerene surface. In the case of $C_{57}Pt_2$ one Pt replaces one C atom of C_{60} and the other Pt replaces a C–C bond, whereas in $C_{56}Pt_2$ each Pt atom replaces one C–C bond. Several geometric factors were studied, three of which have particularly important effects on the relative stability of regioisomers: the Pt–Pt separation, the number of C–C bonds remaining after the substitution and the substituted C–C bond type. All the factors point to the deformation of the fullerene carbon framework as being a general factor that governs the relative stability of the regioisomers. Because of the high number of factors affecting the stability, we used chemometric techniques. Partial Least Squares (PLS) regression was used to establish structure-energy relationships for $C_{57}Pt_2$ and $C_{56}Pt_2$ heterofullerenes. The resulting understanding of the factors that affect the relative isomer stabilities allowed us to predict the stability of larger disubstituted carbon cages, *e.g.* $C_{81}Pt_2$, heterofullerene.

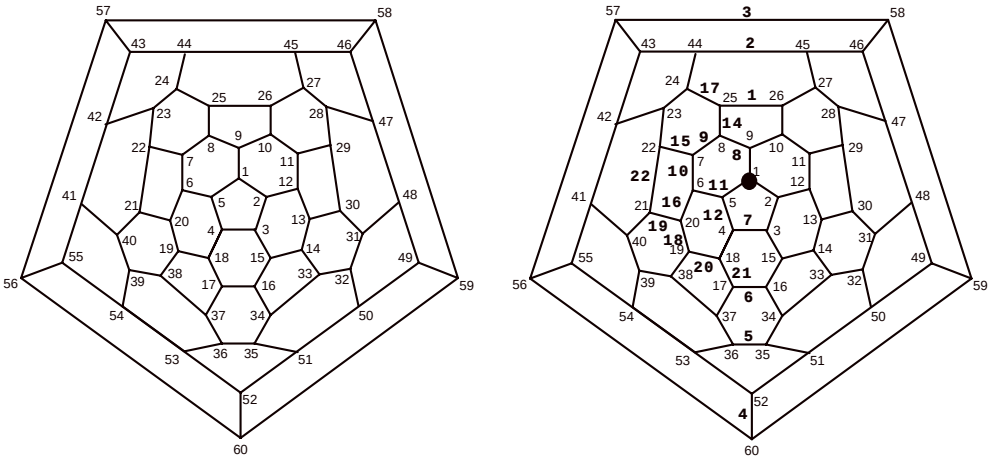

(a) Schlegel diagram of C_{60} (b) Regioisomers of $C_{57}Pt_2$

Figure 5.12 Schlegel diagram showing the numbering system for C_{60} (a) and regioisomers of $C_{57}Pt_2$ (b). The small numbers represent C_{60} numbering. The tricoordinated platinum atom is situated in the black dot. The bigger bold numbers represent the position of the tetracoordinated platinum atom and the regioisomer number. For instance, the regioisomer $C_{57}Pt_2$:**1** is constructed after the substitution of the C1 atom by the first metal and the substitution of C25–C26 bond by the second metal

5.5.1 Regioisomers of $C_{57}Pt_2$

All the carbons in C_{60} are equivalent. As a result, the $C_{59}Pt$ heterofullerene exists as a single isomer with a tricoordinated metal center. The $C_{57}Pt_2$ heterofullerene may be viewed as a derivative of $C_{59}Pt$ in which one of the C–C bonds has been substituted by a second Pt atom. There are 47 different regioisomers for $C_{57}Pt_2$. In these regioisomers one of the Pt atoms is tricoordinated while the other is tetracoordinated. The high number of regioisomers made it necessary to select the isomers to be computed. In the first step, we explored the dependence of the relative stability of the regioisomers on the separation between the two metals. Figure 5.12a shows the numbering system for the carbons in C_{60}. Initially, we consider the series of regioisomers with C_s symmetry [$C_{57}Pt_2$:**1-7**]. In these, one Pt atom replaces the C1 atom and the second Pt atom consecutively replaces the bonds: C25–C26, C44–C45, C57–C58, C52–C60, C35–C36, C16–C17 and

Table 5.13 Description and numbering scheme for regioisomers of $C_{57}Pt_2$

Isomer number	*Symmetry*	*Substituted C–C bonds* [a]	*C–C bond type*
1	*C*s	25,26	6:5
2	*C*s	44,45	6:6
3	*C*s	57,58	6:5
4	*C*s	52,60	6:6
5	*C*s	35,36	6:5
6	*C*s	16,17	6:6
7	*C*s	3,4	6:5
8	C_1	8,9	6:5
9	C_1	7,8	6:6
10	C_1	6,7	6:5
11	C_1	5,6	6:6
12	C_1	4,5	6:5
13	C_1	4,18	6:6
14	C_1	8,25	6:5
15	C_1	7,22	6:5
16	C_1	6,20	6:5
17	C_1	24,25	6:6
18	C_1	19,20	6:6
19	C_1	20,21	6:5
20	C_1	19,20	6:5
21	C_1	17,18	6:5
22	C_1	21,22	6:5

[a] This is the substituted C–C bond which gives a tetracoordinated space to the Pt atom. The tricoordinated Pt atom replaces the C1 atom in all regioisomers.

C3–C4. These regioisomers are represented schematically in the Schlegel diagram of Figure 5.12b as follows: the first Pt atom is represented by a black dot and the second by the position of the isomer number. All the

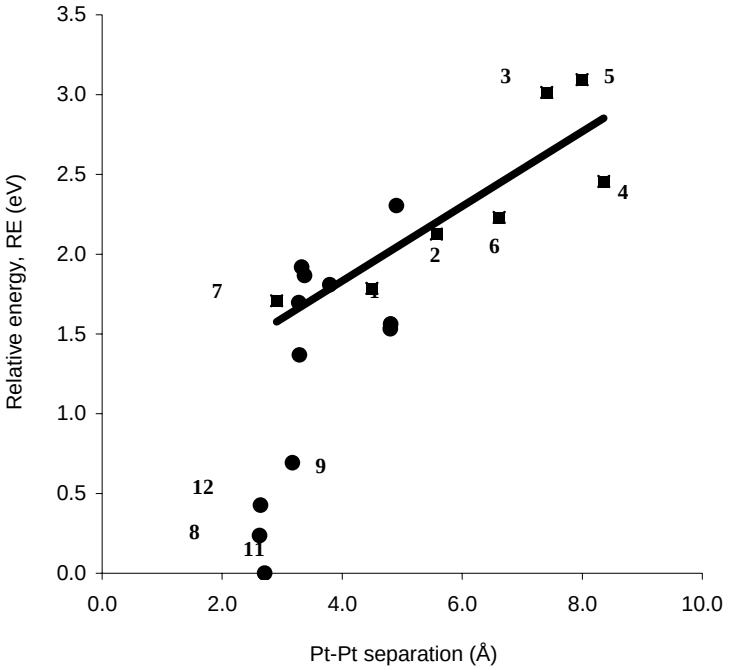

Figure 5.13 Relationship between Pt–Pt separation and stability of the different regioisomers of $C_{57}Pt_2$. The first series of regioisomers, [$C_{57}Pt_2$:**1-7**], are represented by squared dots whereas the rest of regioisomers, [$C_{57}Pt_2$:**8-22**], by circled dots. All regioisomers of the first series are situated in the plot to check the relationship between Pt–Pt separation and isomer stability. $C_{57}Pt_2$:**11** is the most stable regioisomer with Pt–Pt distance of 2.708 Å and the least stable is $C_{57}Pt_2$:**5** with 7.998 Å between both metals. The linear correlation is done with the values of regioisomers [$C_{57}Pt_2$:**1-7**]. Pt–Pt separation and relative energies (REs) for all regioisomers of $C_{57}Pt_2$ are listed in Table 5.17.

regioisomers of $C_{57}Pt_2$ are also tabulated with symmetry, the substituted C–C bond and the C–C bond type in Table 5.13.

Figure 5.13 shows the computed relative energies (RE) of these regioisomers plotted against the Pt–Pt separation in each isomer. The squared dots in Figure 5.13 represent the initial set of seven regioisomers with C_s symmetry. These data show that there is dependence between the

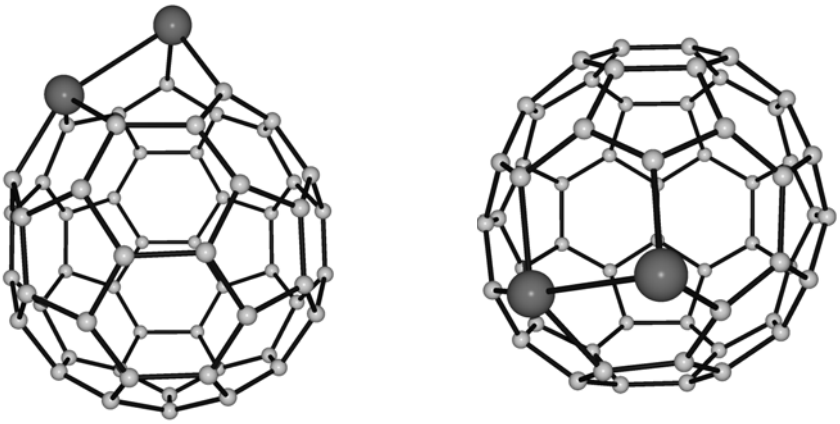

Figure 5.14 Different views of the optimized structure of the most stable $C_{57}Pt_2$:**11** regioisomer.

separation of the heteroatoms and the isomer stability. For example, [$C_{57}Pt_2$:**1** and **7**] regioisomers, which have the two Pt atoms in the same hemisphere, are ~0.8–1.4 eV more stable than the regioisomers in which metals are in different hemispheres of the fullerene: [$C_{57}Pt_2$:**3, 4** and **5**]. Semiempirical studies on heterofullerenes $C_{60-x}Y_x$ (Y = N and B, x = 2-8) and $C_{70-x}Y_x$ (Y = N and B, x = 2-10) also found that the stabilities of the regioisomers decrease as the distance between the heteroatoms increases. It is remarkable that this behavior of the heterofullerenes is clearly different from those found in the exohedral metallofullerenes such as $(\eta^2\text{–}C_{60})\{Pt(PH_3)_2\}_2$ where the double metal addition occurs on opposite ends of the fullerene.[32]

In the second step, each of the C–C bonds in the hemisphere where the first substitution occurs were replaced by a second Pt atom leading to [$C_{57}Pt_2$:**8-22**] regioisomers (Figure 5.12b). These regioisomers retain no symmetry elements. The assumption that substitution in neighbouring sites yields stable structures is fully confirmed. The new [$C_{57}Pt_2$:**8, 11** and **12**] regioisomers have the lowest REs. The most stable regioisomer correspond to the substitution of the 6:6 C–C bond nearest to the previously substituted C1 (C6–C5), $C_{57}Pt_2$:**11** regioisomer, whereas the two next regioisomers, [$C_{57}Pt_2$:**8** and **12**], are those corresponding to the substitution of the 6:5 C–C bond nearest to the previously substituted C1, C8–C9 and C4–C5

respectively. All the regioisomers of $C_{57}Pt_2$ are fully described in Table 5.13. In Figure 5.13, the correlation between Pt–Pt separation and the REs of the regioisomers indicates that this separation will be one of the main factors to govern the stability of the different regioisomers. However, there is no direct correlation between the two variables. The relatively short Pt–Pt distances in the three most stable regioisomers (2.708 Å for $C_{57}Pt_2$:**11**, 2.626 Å for $C_{57}Pt_2$:**8** and 2.643 Å for $C_{57}Pt_2$:**12**, Figure 5.13) suggest the presence of some metal-metal interaction (see below in subsection 5.5.4).

The most stable $C_{57}Pt_2$:**11** regioisomer retains the fullerene structure of C_{60} in the unperturbed hemisphere but some changes are necessary in the substituted hemisphere to accommodate the two Pt atoms. Figure 5.14 shows two views of the optimized structure for $C_{57}Pt_2$:**11** regioisomer. Like $C_{59}Pt$, the tricoordinated-type Pt atom with Pt–C bond lengths of 1.956 Å sticks out from the fullerene surface. The Pt–C distance, 2.025 Å, is somewhat longer for the tetracoordinated-type Pt atom which is located in the fullerene surface in the same way as in $C_{58}Pt$. Heteroatoms such as nitrogen or boron, which replace one single carbon, do not cause such important deformation since the B–C (1.54 Å in $C_{59}B$) and N–C (1.44 Å in $C_{59}N$) bond lengths are more similar to the C–C (1.398 Å for 6:6 and 1.453 Å for 6:5) bond lengths than the Pt–C bond lengths are. The position of the tricoordinated-type Pt atom in $C_{57}Pt_2$ heterofullerene is fully comparable to the situation in $C_{59}M$ (M = Fe, Co, Ni, Rh, Ir, Pt). For example, the computed M–C bond lengths are 1.80 Å in $C_{59}Fe$, 1.81 Å in $C_{59}Co$, in 1.83 Å $C_{59}Ni$, 1.93 Å in $C_{59}Rh$, 1.94 Å in $C_{59}Ir$ and 1.97 Å in $C_{59}Pt$. The significant degree of deformation of the carbon cage in $C_{57}Pt_2$: **11** regioisomer can be appreciated in Figure 5.14.

5.5.2 Regioisomers of $C_{56}Pt_2$

We followed a similar strategy to construct the regioisomers of $C_{56}Pt_2$. When two C_2 units are substituted by two metals the number of possible regioisomers is even larger than in the $C_{57}Pt_2$ heterofullerene. Consequently, we began by exploring the dependence of the isomer stability on the separation of the two tetracoordinated-type Pt atoms. The first nine regioisomers [$C_{56}Pt_2$:**1-9**] incorporate both Pt atoms into the main symmetry plane of C_{60}. These nine structures can be formally separated into two

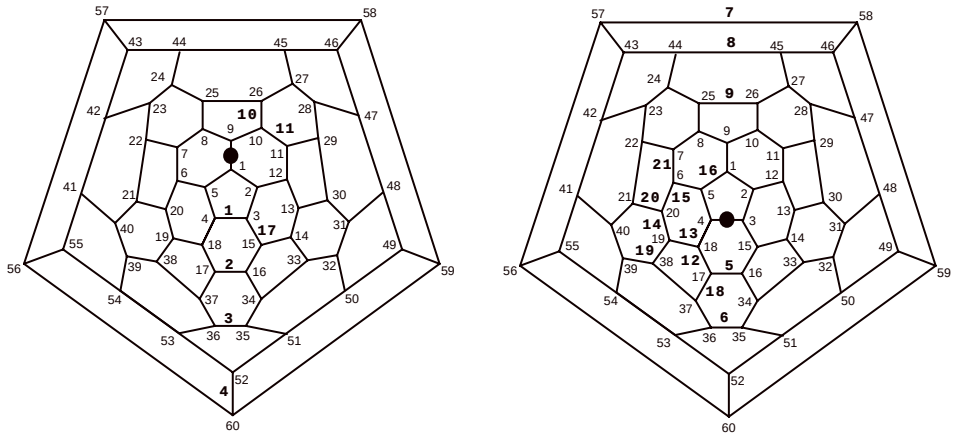

(a) regioisomers of $C_{56}Pt_2$ (b) regioisomers of $C_{56}Pt_2$

Figure 5.15 Schlegel diagram showing the numbering system for regioisomers of $C_{56}Pt_2$. The small numbers represents C_{60} numbering. The first platinum atom is situated in the black dot. In plot on the left (a) the first platinum atom replaces the 6:6 C1–C9 bond whereas in (b) the first platinum atom replaces the 6:5 C3–C4 bond. The bigger bold numbers represent the position of the second metal respect to the first one and also the regioisomer number. For instance, the regioisomer $C_{57}Pt_2$:**10** is constructed after the substitution of the C1–C9 and C10–C26 bonds by two platinum atoms.

subsets: in the first, one Pt replaces the 6:6 C1–C9 bond and a second platinum successively replaces the C_2 units at sites C3–C4, C16–C17, C35–C36 and C52–C60 to produce [$C_{56}Pt_2$:**1-4**] regioisomers. In the second subset, the first heteroatom replaces the 6:5 C3–C4 bond and the second metal successively substitutes the C–C bonds through the symmetry plane without repeating the previous ones to form [$C_{56}Pt_2$:**5-9**] regioisomers. A schematic representation of all these regioisomers is shown in Figure 5.15 and they are fully described in Table 5.14. As in $C_{57}Pt_2$, there is no strict relationship between the Pt–Pt separation and the isomer stability, although in general the destabilization of the cluster increases when the two metals occupy opposite sites in the fullerene. Since the stability of the regioisomers is higher when the two heteroatoms are in the same hemisphere of the fullerene, all the regioisomers of $C_{56}Pt_2$ with a Pt–Pt separation less than 5 Å were constructed and computed. Under this restriction, twelve new additional structures corresponding to substitutions of neighbouring C_2 units

Table 5.14 Description and numbering scheme for regioisomers of $C_{56}Pt_2$

Isomer number	*Symmetry*	*Substituted C–C bonds*	*C–C bond type*
1	C_s	1,9/3,4	6:6/6:5
2	C_s	1,9/16,17	6:6/6:6
3	C_s	1,9/35,36	6:6/6:5
4	D_{2h}	1,9/52,60	6:6/6:6
5	C_s	3,4/17,18	6:5/6:6
6	C_{2v}	3,4/35,36	6:5/6:5
7	C_{2h}	3,4/57,58	6:5/6:5
8	C_s	3,4/44,45	6:5/6:6
9	C_{2v}	3,4/25,26	6:5/6:5
10	C_1	1,9/10,26	6:6/6:5
11	C_s	1,9/10,11	6:6/6:6
12	C_1	3,4/17,18	6:5/6:5
13	C_1	3,4/18,19	6:5/6:5
14	C_1	3,4/19,20	6:5/6:6
15	C_1	3,4/6,20	6:5/6:5
16	C_1	3,4/1,5	6:5/6:5
17	C_s	1,9/3,15	6:6/6:6
18	C_1	3,4/17,37	6:5/6:5
19	C_1	3,4/19,36	6:5/6:5
20	C_s	3,4/20,21	6:5/6:5
21	C_1	3,4/6,7	6:5/6:5

appeared, [$C_{56}Pt_2$:**10-21]** regioisomers, nine of which were non-symmetric structures. The two most stable, [$C_{56}Pt_2$:**10** and **11],** are separated by only 0.037 eV.

Figure 5.16 shows the optimised structure of the most stable $C_{56}Pt_2$:**10** regioisomer. The average Pt–C bond length in $C_{56}Pt_2$:**10** was computed to be 2.042 Å, similar to the Pt–C distances found in the tetracoordinated-type Pt atom of $C_{57}Pt_2$:**11**, 2.025 Å, and $C_{58}Pt$, 2.034 Å. As

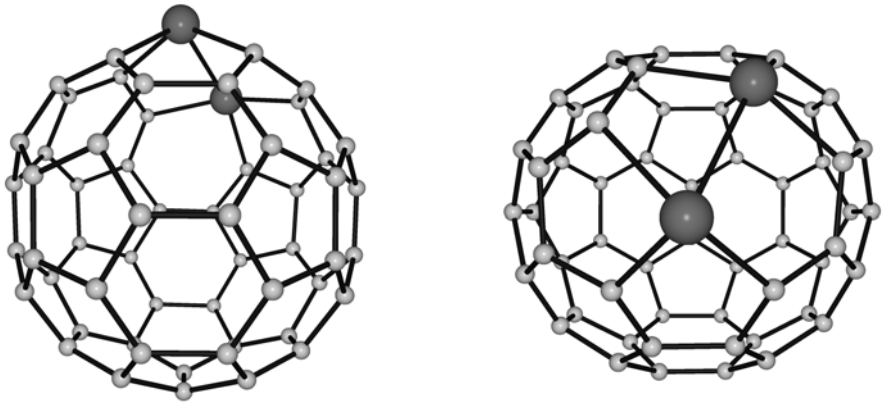

Figure 5.16 Different views of the optimized structure of the most stable $C_{56}Pt_2$:**10** regioisomer.

the views in Figure 5.16 show, the Pt atoms do not protrude far from the fullerene surface. This is also true for the other regioisomers of $C_{56}Pt_2$.

5.5.3 Electronic structure

The SE and BE for mono- and diheterofullerenes are listed in Table 5.15. The values for the monoheterofullerenes were commented in the subsection 5.3.4. When the metal replaces a 6:6 C_2 bond to give $C_{58}Pt + C_2$, the BE involved is 7.35 eV. A subsequent C_2 substitution in $C_{58}Pt$ to give the $C_{56}Pt_2$ diheterofullerene requires a similar amount of energy, more than 6 eV. The analogous process that converts $C_{59}Pt$ to $C_{57}Pt_2$ is less endothermic, 4.88 eV. Hence, in the disubstituted cluster the BE per atom is reduced to −7.16 and −7.19 eV for $C_{56}Pt_2$ and $C_{57}Pt_2$, respectively. Semiempirical studies on B and N heterofullerenes of C_{60} and C_{70}, and DFT calculations on $C_{59}M$ (M = Fe, Co, Ni, Rh) also confirm that when the number of heteroatoms increases the stability is seriously affected.

The ground states of the two most stable regioisomers, [$C_{56}Pt_2$:**10** and **11**], are both singlets with relatively large HOMO-LUMO gaps of *ca.* 0.5 eV. Mulliken charges distinguish the two kinds of metal coordination in $C_{57}Pt_2$:**11**. The net charge for the tricoordinated-type Pt atom is +0.55 *e* whereas for the tetracoordinated-type Pt atoms it is somewhat larger, +0.64 *e*. This trend had already been observed in the $C_{59}Pt$ and $C_{58}Pt$

Table 5.15 Substitution energy (SE) and bonding energy (BE) per atom for mono- and diheterofullerenes [a]

Heterofullerene	*BE* [b]	*Substitution reaction*	*SE* [c]
$C_{59}Pt$	–7.25	$C_{60} + Pt \rightarrow C_{59}Pt + C$	6.20
$C_{58}Pt$	–7.25	$C_{60} + Pt \rightarrow C_{58}Pt + C_2$	7.35
$C_{57}Pt_2$	–7.19	$C_{59}Pt + Pt \rightarrow C_{57}Pt_2 + C_2$	4.88
$C_{56}Pt_2$	–7.16	$C_{58}Pt + Pt \rightarrow C_{56}Pt_2 + C_2$	6.29

[a] Values in eV. [b] BE per atom of the heterofullerene. For C_{60}, the BE was computed to be –7.36 eV. [c] The SE is corrected using the energy of the true atomic groundstate for Pt and C atoms according to reference: Baerends, E. J.; Branchadell, V.; Sodupe, M. *Chem. Phys. Lett.* **1997**, *265*, 481.

monoheterofullerenes: the tetracoordinated Pt atom in $C_{58}Pt$ donates more charge, +0.82 *e*, to the neighbouring C atoms than the tricoordinated Pt atom of $C_{59}Pt$, + 0.76 *e*. The electronic populations of the *s*, *p* and *d* Pt orbitals for the tetracoordinated-type Pt atom of $C_{57}Pt_2$:**11** are 2.66, 6.30 and 8.40 *e*, respectively. These values are quite similar to the electronic populations of the *s*, *p* and *d* Pt orbitals in the tricoordinated-type Pt atoms, 2.65, 6.21, 8.58 *e*, respectively. These values show that Pt donates the electron density through its *d*-orbitals. The Voronoi partition scheme of the electron density suggests that the charge transfer is somewhat greater because this method gives a net charge of +0.95 *e* for the tricoordinated-type Pt atom and +1.10 *e* for the tetracoordinated-type. No significant differences can be seen for the two tetracoordinated-type Pt atoms in the $C_{56}Pt_2$:**10** regioisomer.

As in $C_{59}Pt$ and $C_{58}Pt$, the highest occupied orbitals of $C_{56}Pt_2$:**10** and $C_{57}Pt_2$:**11** regioisomers are formally *d*-metal orbitals. However, in the disubstituted heterofullerenes, the metal-fullerene compounds the *d*-metal orbitals are spread over several molecular orbitals. Specifically, the contribution of the platinum *d* orbitals in $C_{56}Pt_2$:**10** is 26 % in the HOMO and 13 % in the LUMO. For $C_{57}Pt_2$:**11**, the metal contributions to the HOMO and LUMO are 15% and 12%, respectively. Chen and co-workers described these metal-related orbitals for $C_{59}M$ heterofullerenes as defect levels in the C_{60}. This means that heterofullerene orbitals can be seen as the free C_{60} orbitals with a percentage contribution from the metals and, as a result, the electronic structure depends on the incorporated metal.

Nevertheless, it is interesting to note that the energy difference between C-HOMO (the highest carbon-derived occupied orbital) and C-LUMO (the lowest carbon-derived unoccupied orbital) changes very little from one cluster to another and is very close to 1.65 eV, the gap of pure C_{60}. Similar behavior was observed for all the regioisomers of these diheterofullerenes since the C-HOMO/C-LUMO gap appears constant ~1.6 eV.

5.5.4 Metal-metal coupling

The short metal-metal distances found in the most stable regioisomers of $C_{57}Pt_2$ and $C_{56}Pt_2$ heterofullerenes suggest that a significant metal-metal coupling is present. Usually, Pt–Pt bond lengths smaller than 2.6 Å appear in Pt complexes with the metal in low oxidation state. The stabilization produced by the interaction of the two Pt atoms in some heterofullerenes may significantly determine the relative energy of all the regioisomers of $C_{56}Pt_2$ and $C_{57}Pt_2$ heterofullerenes. The mean Pt–Pt distance in the Cambridge Structural Data Base (CSD)[33] for 53 examples, in which Pt atom is tetracoordinated or tricoordinated with a 0 oxidation state, is 2.643 ± 0.045 Å, and the shortest distance is 2.554 Å, which is found in the complex $[Pt_2(\mu\text{-}OPPh_2)(PMePh_2)_2]$ (Refcode JEMLOC [34]). We have regioisomers with a wide range of Pt–Pt distances, from 2.626 Å to 8.358 Å in $C_{57}Pt_2$ and from 2.683 Å to 7.750 Å in the $C_{56}Pt_2$ heterofullerene. The Pt–Pt coupling has been investigated only in the regioisomers with metal-metal distances shorter than 3 Å. The molecular orbital analysis does not make it possible to draw conclusions about the nature of the metal-metal interaction because the Pt *d* orbitals are spread into multiple molecular orbitals. The topological analysis of the total charge density function has proved to be a powerful tool in determining the bonding character in several kinds of bonds.[35] According to the theory of Atoms in Molecules, the presence of a (3,–1) bond critical point (bcp) linking two atoms is a *sufficient* condition for the presence of the bond. Our experience with transition-metal compounds shows that the lack of a bond critical point linking two transition metals does not exclude the existence of metal-metal interactions. For example, a critical point was not detected between the titanium atoms in Ti_8C_{12} but there is a clear metal-metal interaction.[36] On the other hand, the characterization of a bcp between two transition-metal

Table 5.16 Several parameters for determining the bonding character of the platinum-platinum bond

Isomer number	*Pt–Pt* [a]	*Critical point*	*Number of Pt–C bonds* [b]	*Sum of Mulliken net charges of both Pt*
$C_{57}Pt_2$				
8	2.626	(3, –1)	2,3	1.168
12	2.643	(3, –1)	2,3	1.132
11	2.708	(3, –1)	2,3	1.189
7	2.905	(3,1)	3,4	1.608
9	3.171	(3,1)	3,4	1.564
3	7.408	--	3,4	1.588
$C_{56}Pt_2$				
1	2.683	(3,1)	4,4	1.583
16	2.683	[c]	3,3	1.301
5	2.700	(3,1)	4,4	1.583
13	2.714	(3, –1)	3,3	1.240
10	2.739	(3, –1)	3,3	1.249
11	2.836	(3, –1)	3,3	1.162
12	2.847	(3, –1)	3,3	1.124
18	2.856	(3,1)	4,4	1.514
14	2.863	(3,1)	4,4	1.469
15	2.866	(3,1)	4,4	1.526
3	7.071	--	4,4	1.654

[a] Pt–Pt separation in Å. [b] Number of Pt–C bonds with a distance shorter than 2.212 Å. In the regioisomers of $C_{57}Pt_2$, the first number refers to the tricoordinated-type Pt atom and the second number to the tetracoordinated type. In the regioisomers of $C_{56}Pt_2$, both platinum atoms are tetracoordinated. [c] No critical point was localized in regioisomer $C_{56}Pt_2$:**16** but a (3, –1) bcp is expected.

atoms is strong evidence of the coupling. Bonding and charge properties for these regioisomers and some others are given in Table 5.16 for purposes of comparison.

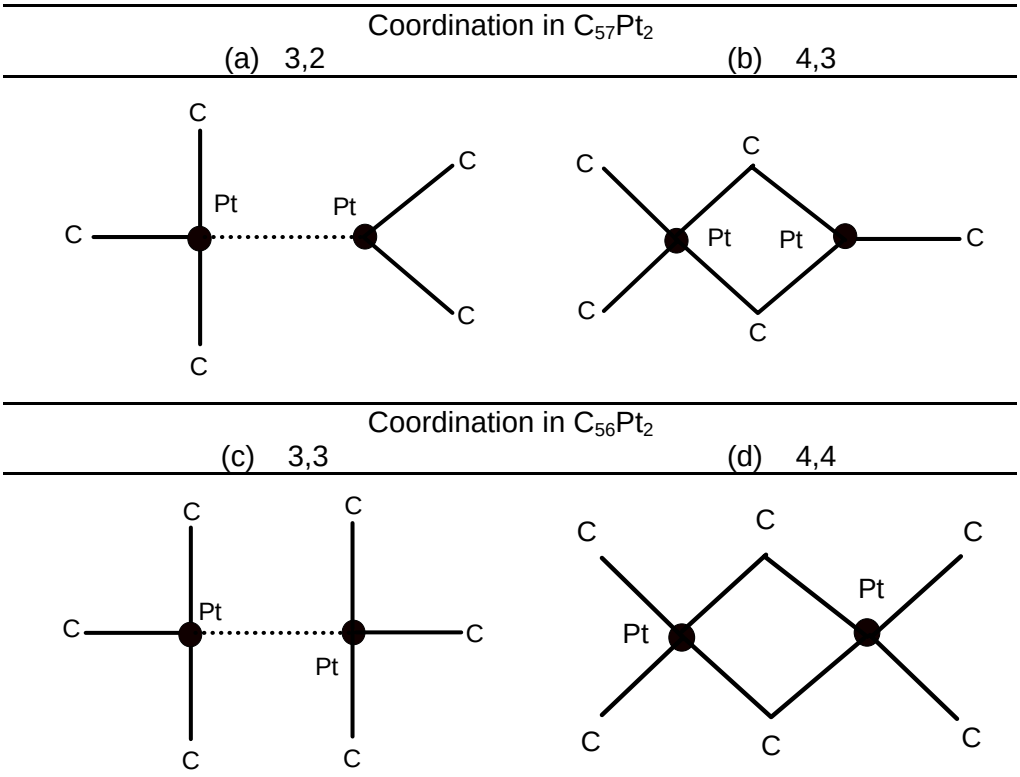

Figure 5.17 Schematic representation of the platinum atoms coordination in regioisomers of $C_{57}Pt_2$ and $C_{56}Pt_2$ that the platinum-platinum distance is lower than 3 Å. Scheme (a) with a platinum surrounded by three carbons and the other by two (3,2) corresponds to regioisomers [$C_{57}Pt_2$:**8**, **11** and **12**] and scheme (b) corresponds to regioisomers [$C_{57}Pt_2$:**7** and **9**]. Scheme (c) and (d) correspond to $C_{56}Pt_2$ heterofullerenes, regioisomers [$C_{56}Pt_2$:**10, 11**, **12** and **13**] and regioisomers [$C_{56}Pt_2$:**1**, **5**, **14**, **15** and **18**], respectively.

In $C_{57}Pt_2$, bonding critical points were found to link the Pt atoms for the three regioisomers with the shortest Pt–Pt separation, [$C_{57}Pt_2$:**8**, **11** and **12**] (Table 5.16). In these clusters, the presence of the bcp coincides with a low Pt coordination number. As seen in Figure 5.17, one of the metals is coordinated to three C atoms and the other to two C atoms (coordination 3,2 in Figure 5.17). In all other regioisomers, the Pt atoms are coordinated to four and three C atoms (coordination 4,3) and the result is the lack of any metal-metal interaction. In $C_{57}Pt_2$:**7** regioisomer, which has a relatively short

Pt–Pt distance of 2.905 Å, a (3,+1) critical point that denotes the absence of metal-metal interaction was found in the region between the two metals. Mulliken net charges can also provide some clues about the metal coupling. According to the sum of net charges of both metals, there are two groups of heteroatoms: one group with a positive charge of +1.2 *e* corresponds to the metals for which a bcp was characterized. In all other isomers the metals have somewhat larger net charges, between +1.5 and +1.6 *e*. The low depopulation of the platinum orbitals in [$C_{57}Pt_2$:**8**, **11** and **12**] regioisomers permits a concentration of the electronic density in the intermetallic region, and this is another indication of a metal-metal interaction in these clusters.

The situation in $C_{56}Pt_2$ is not so simple. There are 10 regioisomers with a Pt–Pt distance shorter than 3 Å. In five of them, [$C_{56}Pt_2$:**10**, **11**, **12**, **13** and **16**], both platinum atoms are surrounded by three C atoms (coordination 3,3 in Figure 5.17), whereas in the other structures the metal is coordinated to four C atoms (coordination 4,4). The presence of a direct Pt–Pt interaction is only expected for coordination 3,3. Indeed, the bcp linking the two Pt atoms is only characterized for isomers with this low coordination, [$C_{56}Pt_2$:**10, 11, 12** and **13**] (Table 5.16). It is worth mentioning that for isomer $C_{56}Pt_2$:**16**, which has a 3,3 coordination and a short Pt–Pt distance of 2.683 Å, it was not possible to characterize the expected bcp, even though an accurate search was made. In all these structures, the Mulliken charges follow the same tendency as that observed for $C_{57}Pt_2$: the group of Pt atoms characterized by a low coordination and by the presence of Pt–Pt interaction produces a smaller charge transfer to the fullerene carbon framework.

5.5.5 Topological and structural factors that govern isomer stability

The substitution of several C atoms in a fullerene produces a high number of possible regioisomers and computations on all of these become unrealistic as the size of the fullerene increases. Therefore, it is necessary to know which factors determine the isomer stability and to have some information about how to search for the most stable structures in any substituted fullerene. Kurita et al.[37] have already pointed out that the electronic properties of $C_{58}X_2$ (X = B, N) largely depend on the relative positions of the heteroatoms in the heterofullerenes. Furthermore, they

presented a systematic search which found the most stable isomer for $C_{58}X_2$ using semiempirical methods.[38] If we know a priori where to look for the most stable structures of heterofullerenes, we will be able to save a huge amount of the computational effort involved in predicting electronic properties.

The most important factors that have an effect on the stability of $C_{57}Pt_2$ and $C_{56}Pt_2$ are listed in Tables 5.17 and 5.18, respectively. We classified them into topological and structural factors. The topological factors are those which provide constitutive information about each regioisomer and can be determined or estimated a priori without any calculation. Topological factors are the Pt–Pt separation, the number of C–C bonds, the substituted C–C bond type and the number of heterorings. These factors are listed in the third to sixth columns in Table 5.17 and 5.18. The structural factors are determined once the geometry of the molecules is fully determined and characterize the geometry of each regioisomer in detail. The structural factors considered here are: cage radius, average bond lengths (Pt–C, 6:6 C–C and 6:5 C–C) and HOMA index (a geometric parameter of aromaticity). These factors are listed in the last five columns of Table 5.17 and 5.18. Below we discuss the topological factors first and then the structural factors.

Pt–Pt separation. The incorporation of one metal in the fullerene cage requires a hole to be made in the carbon cage. When two metals are close together, only one hole is necessary in the dimetallic heterofullerenes and this situation is energetically more favorable than the double perforation of the carbon skeleton that occurs when, for example, the two metals are in different hemispheres. The regioisomers of $C_{57}Pt_2$ with a bonding Pt–Pt distance, [$C_{57}Pt_2$:**8**, **11** and **12**], are the most stable structures whereas the regioisomers with a Pt–Pt separation longer than 5 Å are more than 2 eV less stable (Figure 5.13 and Table 5.17). The longest Pt–Pt separation is found in the $C_{57}Pt_2$:**4** regioisomer, 8.358 Å, which is 2.456 eV less stable than $C_{57}Pt_2$:**11**. For regioisomers of $C_{56}Pt_2$, the correlation is not so high but the Pt–Pt distances of the first seven most stable regioisomers are shorter than 3 Å. Although, a priori, we do not know the exact value of Pt–Pt separation, this factor has been classified as topological due to the fundamental information that it gives about the regioisomers and moreover it can be estimated approximately. In fact, Pt–Pt separation has been the

guide to construct all regioisomers of $C_{57}Pt_2$ and $C_{56}Pt_2$ in the previous sections and it is one of the most important factors affecting the relative stability.

Number of C–C bonds. Not all regioisomers have the same number of C–C and Pt–C bonds. Structures with metal-metal contacts have more C–C bonds, although are correspondingly fewer Pt–C bonds. We have checked that it is preferred to maintain the number of C–C before creating Pt–C bonds. So, all regioisomers of $C_{57}Pt_2$ have 82 C–C bonds and 7 Pt–C bonds except the three most stable ones, [$C_{57}Pt_2$:**8, 11** and **12**], which have 83 C–C bonds, 5 Pt–C bonds and one Pt–Pt bond. Regioisomers of $C_{56}Pt_2$ can be divided into two groups: the group, [$C_{56}Pt_2$:**10**, **11**, **12**, **13** and **16**], has one metal-metal bond, 81 C–C bonds and 6 Pt–C bonds and the rest of the regioisomers have just 80 C–C bonds and 8 Pt–C bonds.

Substituted C–C bonds. Previous calculations for the monosubstituted $C_{58}Pt$ and $C_{58}Ir$ heterofullerenes showed that the substitution of a 6:5 C–C bond by a metal instead of a 6:6 C–C bond is disfavoured by 0.58 eV for Pt and 0.61 eV for Ir. This trend is also found for $C_{57}Pt_2$ and $C_{56}Pt_2$ heterofullerenes. Of the three most stable structures of $C_{57}Pt_2$, [$C_{57}Pt_2$:**8, 11** and **12**] regioisomers, the most stable, $C_{57}Pt_2$:**11**, corresponds to a 6:6 C–C bond substitution. Again, the most stable regioisomers of the group with intermediate relative energy and medium Pt–Pt distance are those with a 6:6 C–C bond substitution, [$C_{57}Pt_2$:**9**, **13**, **17** and **18**] regioisomers. This trend is also observed for the regioisomers with the longest Pt–Pt distances. The most stable are [$C_{57}Pt_2$:**2** and **6**] regioisomers, which Pt atom substitutes a 6:6 C–C bond. $C_{57}Pt_2$:**4** regioisomer is a good example that isomer stability is a compromise of different factors. Following the observed trends, the 6:6 C–C bond substitution stabilizes the isomer, while the large Pt–Pt distance increases instability. As a whole, $C_{57}Pt_2$:**4** is less stable than $C_{57}Pt_2$:**19**, which has a substitution of a 6:5 C–C bond but the distance Pt–Pt is much shorter. In regioisomers of $C_{56}Pt_2$, both platinum atoms are tetracoordinated and come from a C_2 substitution. The second most stable $C_{56}Pt_2$:**11** regioisomer, which is only 0.037 eV higher in energy, has two 6:6 C–C bond type substitutions,

although the most stable regioisomer $C_{56}Pt_2$:**10** has just one 6:6 C–C bond type substitution. Of the group of regioisomers which have only 80 C–C bonds, the most stable are those that have 6:6 C–C bond type substitutions, [$C_{56}Pt_2$:**1, 2, 4, 5, 14** and **17**], and the least stable are those that have only 6:5 C–C bond type substitutions, such as [$C_{56}Pt_2$:**6, 7, 19, 20** and **21**].

Heterorings. The number of rings with a heteroatom incorporated — referred to *heterorings*— is also a topological factor. This parameter gives an indirect measure of the carbon skeleton change and it is closely related to the metal-metal distance. The regioisomers with the fewest heterorings (5 in $C_{57}Pt_2$ and 4 in $C_{56}Pt_2$) tend to have the shortest metal-metal distances and in consequence the lower REs. If both substitutions occur at opposite hemispheres of the fullerene the number of heterorings increases to 7 in $C_{57}Pt_2$ and 8 in $C_{56}Pt_2$ and the destabilization also increases.

Structural factors. The structural factors are obtained after the geometry optimization of each regioisomer. The cage radius characterizes the geometric structure of each regioisomer. At the present level of theory, the cage radius for C_{60}, $C_{59}Pt$, $C_{58}Pt$ and $C_{58}Pt$ is computed to be 3.551 Å, 3.580 Å, 3.562 Å and 3.569 Å, respectively. We obtained a cage radius of around 3.587 Å for $C_{57}Pt_2$:**11** and somewhat smaller for $C_{56}Pt_2$:**10**, 3.575 Å. For structural factors we also took into account the average bond lengths of all Pt–C distances, 6:6 C–C distances and 6:5 C–C distances, because short bond lengths could lead to special stabilization in regioisomers. Finally, our study also includes a structure-based measure of aromaticity: the HOMA index. The HOMA value calculated at the present level of computation for reference systems such as benzene, C_{60}, $C_{59}Pt$, $C_{58}Pt$ and $C_{58}Pt$ were computed to be 0.969, 0.274, 0.268, 0.279 and 0.240, respectively. For purposes of comparison, more HOMA values for polycyclic aromatic hydrocarbons can be found in ref. [39]. The values for the regioisomers of the disubstituted species of C_{60} range between 0.20 and 0.31. The second least stable regioisomer of $C_{56}Pt_2$, $C_{56}Pt_2$:**7**, has the less aromatic HOMA value (0.205) and the second most stable regioisomer, $C_{56}Pt_2$:**11**, has the most aromatic HOMA value (0.310).

Table 5.17 Geometric factors and relative energies (REs) for regioisomers of $C_{57}Pt_2$ [a]

Iso.	*RE*	*Topological factors*				*Structural factors*				
		Pt–Pt	*No. C–C bonds*	*C–C bond type*	*Hete-ro-rings*	*Cage radius*	*Pt–C*	*6:6 C–C*	*6:5 C–C*	*HOMA* [b]
C_{60}		--	90	--	--	3.551	--	1.398	1.453	0.274
$C_{59}Pt$		--	87	--	3	3.580	1.982	1.400	1.452	0.268
$C_{58}Pt$	0.000	--	85	6:6	4	3.562	2.034	1.403	1.451	0.279
	0.630	--	85	6:5	4	3.569	2.031	1.400	1.453	0.240
11	0.000	2.708	83	6:6	5	3.587	1.997	1.400	1.451	0.279
8	0.237	2.626	83	6:5	5	3.592	1.999	1.400	1.452	0.263
12	0.426	2.643	83	6:5	5	3.592	2.007	1.399	1.452	0.259
9	0.692	3.171	82	6:6	6	3.591	2.028	1.400	1.451	0.285
13	1.368	3.289	82	6:6	7	3.598	2.030	1.403	1.451	0.313
17	1.531	4.806	82	6:6	7	3.593	2.025	1.401	1.450	0.287
18	1.562	4.809	82	6:6	7	3.590	2.020	1.403	1.450	0.304
10	1.696	3.280	82	6:5	6	3.595	2.020	1.399	1.452	0.265
7	1.708	2.905	82	6:5	7	3.595	2.005	1.401	1.452	0.237
1	1.787	4.493	82	6:5	7	3.596	2.024	1.399	1.452	0.263
15	1.808	3.792	82	6:5	6	3.606	2.034	1.398	1.452	0.271
14	1.866	3.376	82	6:5	6	3.602	2.024	1.401	1.451	0.283
16	1.917	3.327	82	6:5	6	3.605	2.022	1.402	1.451	0.276
2	2.126	5.566	82	6:6	7	3.590	2.012	1.405	1.450	0.276
6	2.230	6.614	82	6:6	7	3.590	2.012	1.404	1.449	0.284
4	2.456	8.358	82	6:6	7	3.591	2.011	1.405	1.451	0.273
19	2.303	4.903	82	6:5	7	3.598	2.021	1.399	1.450	0.269
21	2.624	4.837	82	6:5	7	3.599	2.019	1.404	1.451	0.271
20	2.765	4.762	82	6:5	7	3.598	2.015	1.401	1.452	0.257
22	2.912	5.193	82	6:5	7	3.600	2.010	1.403	1.452	0.241
3	3.014	7.408	82	6:5	7	3.599	2.012	1.402	1.452	0.238
5	3.094	7.998	82	6:5	7	3.599	2.012	1.402	1.452	0.243

[a] Distances in Å. [b] Taking into account only C–C bonds. For these bonds, calculated with $\alpha = 257.7$ and $R_{opt} = 1.388$ according to reference 24.

Table 5.18 Geometric factors and relative energies (REs) for regioisomers of $C_{56}Pt_2$ [a]

Iso. Num.	*RE*	*Topological factors*				*Structural factors*				
		Pt–Pt	*No. C–C bonds*	*C–C bond type*	*Hetero-rings*	*Cage radius*	*Pt–C*	*6:6 C–C*	*6:5 C–C*	*HOMA* [b]
10	0.000	2.739	81	6:6/6:5	4	3.575	2.042	1.401	1.451	0.287
11	0.037	2.836	81	6:6/6:6	4	3.568	2.046	1.401	1.450	0.310
13	0.200	2.714	81	6:5/6:5	4	3.583	2.041	1.400	1.452	0.278
16	0.789	2.683	81	6:5/6:5	4	3.573	2.010	1.399	1.453	0.230
12	1.083	2.847	81	6:5/6:5	4	3.581	2.032	1.400	1.452	0.288
5	0.123	2.700	80	6:6/6:5	6	3.573	2.042	1.403	1.451	0.296
1	0.911	2.683	80	6:6/6:5	6	3.578	2.058	1.402	1.451	0.298
2	0.943	5.488	80	6:6/6:6	8	3.571	2.038	1.405	1.449	0.310
17	1.048	3.429	80	6:6/6:6	6	3.582	2.054	1.403	1.449	0.304
14	1.123	2.863	80	6:5/6:6	6	3.582	2.074	1.399	1.449	0.318
4	1.267	7.750	80	6:6/6:6	8	3.575	2.038	1.408	1.451	0.281
15	1.584	2.866	80	6:5/6:5	6	3.587	2.066	1.400	1.451	0.300
18	1.589	2.856	80	6:5/6:5	6	3.587	2.068	1.400	1.451	0.294
3	1.776	7.071	80	6:6/6:5	8	3.581	2.036	1.406	1.453	0.247
8	1.887	7.290	80	6:5/6:6	8	3.581	2.036	1.405	1.452	0.241
6	2.152	5.395	80	6:5/6:5	8	3.582	2.038	1.401	1.452	0.238
19	2.156	3.667	80	6:5/6:5	6	3.594	2.051	1.401	1.452	0.243
21	2.271	3.664	80	6:5/6:5	6	3.579	2.050	1.401	1.453	0.231
9	2.399	5.959	80	6:5/6:5	8	3.584	2.034	1.401	1.453	0.214
7	2.481	7.729	80	6:5/6:5	8	3.590	2.033	1.402	1.454	0.205
20	2.723	4.135	80	6:5/6:5	6	3.598	2.059	1.400	1.451	0.268

[a] Distances in Å. [b] Taking into account only C–C bonds. For these bonds, calculated with $\alpha = 257.7$ and $R_{opt} = 1.388$ according to reference 24.

5.5.6 Chemometric study of the structure-energy relationship

Although the analysis of each topological factor and the relative energy showed some relevant trends, the relationship between the structural factors and the stability is less clear. Actually, none of the nine factors by itself can satisfactorily explain the order of the relative energy or the groups of regioisomers observed according to their structure-energy relationship. Hence we decided to investigate the simultaneous (multivariate) relationship among the nine factors and the relative energy using Partial Least Squares (PLS) regression. This multivariate data analysis technique, which has become very popular in chemometrics in the past years,[40] will search for the combinations of the topological/structural factors (*x*-variables) that best explain the relative energy (*y*-variable). Each combination is called a latent variable (LV). The first latent variable (LV1) describes the largest part of the *x*-variables that has the highest correlation with the relative energy. The second latent variable (LV2) describes the largest part of the variability left over by LV1, and so on. The latest latent variables describe non-useful variation and can be discarded. Hence, by considering only the first few latent variables we can study trends between the nine original factors/*x*-variables and the relative energy without being blurred by the redundancy in the data.

The exploratory analysis using PLS regression was first applied to the data in Table 5.17. In order to prepare the data for the analysis, the variable C–C bond type was coded as 1 and 0, corresponding to 6:6 and 6:5 respectively. Then all the *x*-variables were autoscaled so that each variable had the same *a priori* importance in the calculation of the model.

Figure 5.18 shows the two-dimensional biplot (LV1 versus LV2) for regioisomers of $C_{57}Pt_2$. The plot shows 60 % of the original *x*-data, which are correlated to 95% of the *y*-data. This means that 40% of the *x*-data is not relevant for describing the relative energy. Each regioisomer is indicated by a dot. Its position depends on the values of the *x*-variables. Two regioisomers are close to each other when they have similar values of the original *x*-variables. Their separation is large when they have very different values of the *x*-variables. Each *x*-variable is indicated by an arrow, which points to the direction of increasing values of that variable.

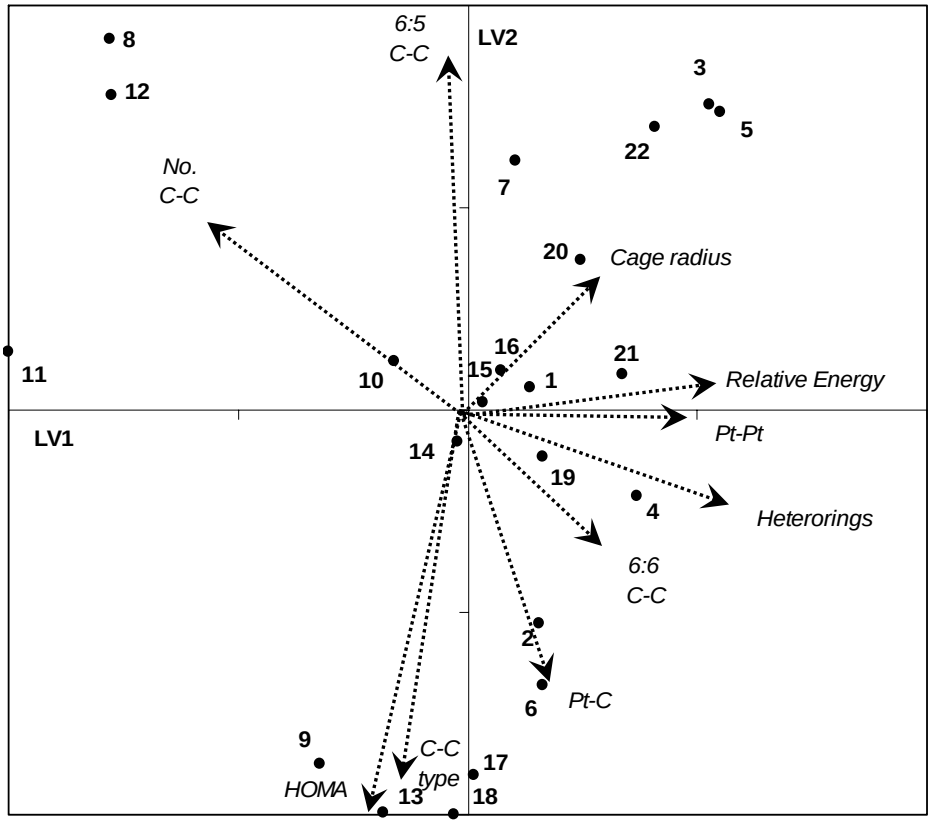

Figure 5.18 *Biplot* for regioisomers of $C_{57}Pt_2$ obtained after PLS regression on the nine factors of Table 5.17. Dots represent regioisomers and arrows represent factors. The plot shows 60 % of the *x*-data, which are correlated to 95 % of the *y*-data.

By considering regioisomers and original variables together, we can visually find similarities and differences among regioisomers and study what variables are responsible for such interdependencies, thus obtaining chemical/structural information. The arrow of the relative energy points in the direction of the positive values of LV1 (abscissa axis). Hence, LV1 discriminates the regioisomers in decreasing order of stability from left to right: [$C_{57}Pt_2$:**8**, **11** and **12**], on the far left, are the most stable and [$C_{57}Pt_2$:**3, 5** and **22**], on the far right, are the least stable. By considering the arrows of

the *x*-variables that are most parallel to LV1, we note that stability is mainly characterized by the combined effect of a short Pt–Pt separation, a small number of heterorings and a large number of retained C–C bonds. [$C_{57}Pt_2$:**8**, **11** and **12**] regioisomers have 83 C–C bonds, 5 heterorings and the shortest Pt–Pt separation. The regioisomers with less C–C bonds, a longer Pt–Pt separation and more heterorings are on the right. The other six variables contribute to the stability to a smaller extend. HOMA, C–C bond type and 6:5 C–C bond lengths are responsible for position of the regioisomers at the top and the bottom of the plot. As we move down-left, the regioisomers have higher aromatic HOMA values, 6:6 C–C substitution and a low 6:5 C–C distance. The combined effect of these three factors also makes the regioisomers more stable. For example, $C_{57}Pt_2$:**11** regioisomer is down-left compared to [$C_{57}Pt_2$:**8** and **12**] regioisomers, which have smaller HOMA values, 6:5 C–C bond substitution and larger 6:5 C–C distances. The same trend can be observed with [$C_{57}Pt_2$:**9**, **13**, **17** and **18**] regioisomers with respect to [$C_{57}Pt_2$:**1**, **7**, **10**, **14**, **15** and **16**], and [$C_{57}Pt_2$:**2**, **4** and **6**] regioisomers with respect to [$C_{57}Pt_2$:**3**, **5**, **19**, **20**, **21** and **22**]. It is a quite important conclusion that will be studied later: the removal of 6:6 C–C bonds affect less the aromaticity of the cage than the removal of 6:5 C–C bonds. As far the cage radius, Pt–C distance and 6:6 C–C bond lengths are concerned, a high value increases instability of the regioisomers. This is to be expected for cage radius since a high value of this parameter indicates more distortion.

The regression coefficients of the PLS model (Table 5.19) give a quantitative measure of the relative importance of each *x*-variable in defining the stability of the regioisomers. A positive sign indicates that an increase in the value of the *x*-variable increases the relative energy. A negative sign indicates the contrary effect. The sign agrees with the trends observed in the biplot. Based on the magnitude of these coefficients we can distinguish three groups.

The largest regression coefficients are those of the topological factors: Pt–Pt separation, the number of heterorings and number of retained C–C bonds. The Pt–C and the 6:5 C–C bond lengths are the two least important factors and the rest of the factors have an intermediate impact on the relative stability in the order: Cage radius > HOMA > 6:6 C–C bond lengths. This result is quite significative, since it suggests that the

Table 5.19 Regression coefficients of PLS model considering two latent variables

Factor		$C_{57}Pt_2$	$C_{56}Pt_2$
Topological	Pt–Pt	0.258	0.150
	No. C–C bonds	–0.218	–0.247
	C–C bond type	–0.134	–0.183
	No. Heterorings	0.258	0.201
Structural	Cage radius	0.179	0.307
	Pt–C	0.024	0.106
	6:6 C–C	0.152	–0.055
	6:5 C–C	0.023	0.104
	HOMA	–0.159	–0.200

topological factors by themselves can almost estimate the relative energy of regioisomers of $C_{57}Pt_2$. Actually we can compare the ability of the PLS model for predicting the relative energy in terms of the average error of the predictions. This value is given by the root mean squared error of prediction (RMSEP) calculated by cross-validation. The model calculated with the nine *x*-variables has a RMSEP of 0.233 eV while the model calculated considering only the four topological factors has a RMSEP of 0.288 eV. This result suggests that considering the remaining factors the prediction is only improved slightly. In both cases, average errors of 0.233 eV or 0.288 eV are low enough compared to the relative energy values range (from 0 to 3.094) to enable trends to be observed just from the predictions using the geometric parameters of the molecule. The accomplishment of the prediction is clearly shown in the plot of DFT calculated versus PLS predicted REs (Figure 5.19).

The PLS analysis was also applied to the $C_{56}Pt_2$ data in Table 5.18. Data were handled as in the PLS analysis of Table 5.17 except that, in this case, the variable C–C bond type was coded as 0, 1 and 2. The biplot is shown in Figure 5.20. The trends observed in the structure-energy relationship are similar to those seen for regioisomers of $C_{57}Pt_2$ although the difference between topological and structural factors is not so marked and the prediction of relative stability for $C_{56}Pt_2$ is less accurated (the PLS model of two latent variables yields a RMSEP of 0.379 eV). The number of C–C bonds, and the number of heterorings are still highly related to the relative energy but, in this case, Pt–Pt distance is not so related to a higher stability

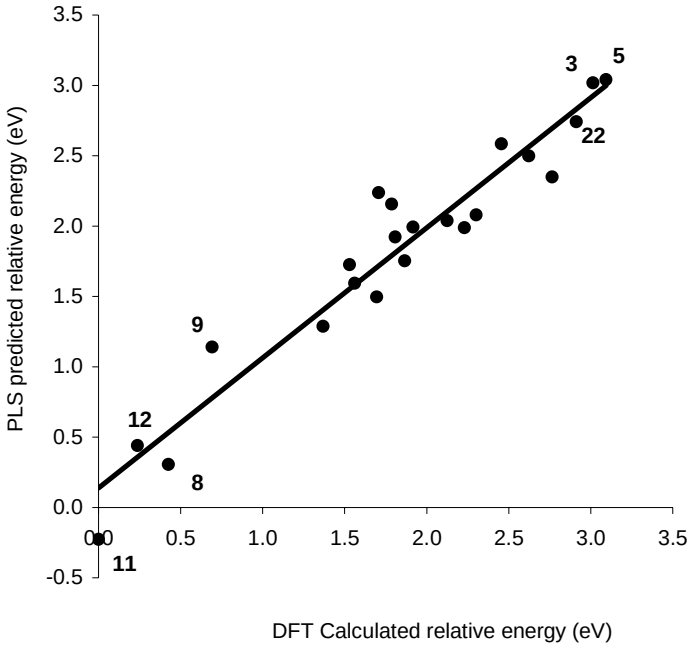

Figure 5.19 DFT calculated versus PLS predicted relative energy (RE) obtained from the PLS regression model on the nine studied factors of $C_{57}Pt_2$. Only the most stable and least stable regioisomers are labeled.

while the cage radius and HOMA confirm their correlation to the stability of heterofullerenes (Table 5.19). We also realise that the Pt–C, 6:6 C–C and 6:5 C–C bond lengths have an ambiguous and weak correlation to the stability of heterofullerenes and thus these factors are not important for describing stability of heterofullerenes. This trend was also found in $C_{57}Pt_2$ analysis.

5.5.7 Stability of the carbon skeleton is the principal factor that determines the isomer stability

Without a doubt, the PLS technique enables us to find structure-energy relationships and it has proved to be valid for analysing multivariate data. Apart from the stabilization produced by the weak metal coupling detected in some regioisomers, the factors that dominate the structure-

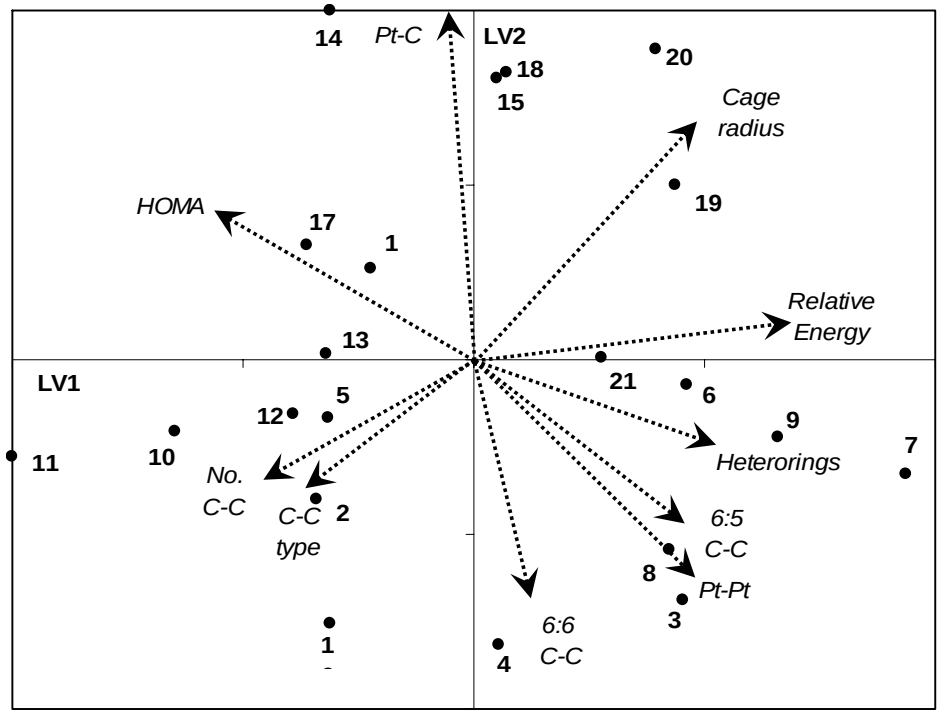

Figure 5.20 *Biplot* for regioisomers of $C_{56}Pt_2$ obtained after PLS regression on the nine factors of Table 5.18. Dots represent regioisomers and arrows represent factors. The plot shows 60 % of the x-data, which are correlated to 86 % of the y-data.

energy relationship are practically independent of the metal. In fact, the relative energy seems to be a measure of the distortion of the cage skeleton from the free equilibrium geometry produced by the inclusion of both metal atoms. So the Pt–Pt separation, the number of C–C bonds, the substituted C–C bond type, the number of heterorings, cage radius, the different bond lengths and the HOMA index are closely related and interdependent because they are all simply indirect measurements of this distortion. To confirm that the REs of the various regioisomers are independent of the metal incorporated, first we changed the number of electrons in several regioisomers of $C_{56}Pt_2$ calculating the cation, $C_{56}Pt_2^+$, and anion, $C_{56}Pt_2^-$ species (Table 5.20). The regioisomers selected for the test are some of the most symmetric regioisomers from the groups with high, [$C_{56}Pt_2$:**10** and **11**],

Table 5.20 Relative energies (REs) for different clusters: $C_{56}Pt_2$, $C_{56}Pt_2^+$, $C_{56}Pt_2^-$, $C_{56}Ti_2$ and C_{56} [a]

Isomer number	$C_{56}Pt_2$	$C_{56}Pt_2^+$	$C_{56}Pt_2^-$	$C_{56}Ti_2$	C_{56}
10	0.00	0.00	0.00	0.00	0.00
11	0.04	–0.09	0.15	0.57	–1.06
2	0.94	1.07	0.75	1.06	2.27
4	1.27	1.27	1.04	1.40	2.58
6	2.15	2.27	2.17	2.35	4.07
9	2.40	2.38	2.57	2.58	4.14
7	2.48	2.59	2.58	3.08	4.25

[a] Values in eV.

intermediate, [$C_{56}Pt_2$: **2** and **4**], and low, [$C_{56}Pt_2$:**6, 7** and **9**], stability. The positive charge is localized basically in both platinum atoms rather than in the fullerene carbon framework: for instance, the sum of the Mulliken net charge of both Pt atoms in $C_{56}Pt_2$:**10** was computed to be 1.249 *e* and in the analogue cation 1.333 *e*. Despite the repulsion between both charges, the relative stability of the various regioisomers does not change (Table 5.20). The anion spreads all the additional charge over the fullerene carbon framework and also retains the relative energy of the neutral platinum analog. Secondly, the incorporation of another metal such as titanium was also tested without changing the order of the relative energy but increasing the REs among regioisomers. A Ti atom behaves like a Pt atom in the $C_{56}Pt_2$ heterofullerene because the computed Ti–C bond length is very similar to Pt–C in $C_{56}M_2$ heterofullerenes, 2.098 Å versus 2.042 Å for $C_{56}M_2$:**10**.

Finally, single point calculations were carried out by extracting Pt atoms from the optimized $C_{56}Pt_2$ structures. In that case we analyse the effect of having a hole in the stabilization of the rest of carbon skeleton. Determining the electronic state of fullerenes with holes is not easy because of the presence of dangling bonds. The lowest electronic state of holed C_{58} fullerene formed from C_{60} by removal of 6:6 C–C bond type is a triplet but when two C_2 units are removed to form C_{56} the singlet competes with the triplet for the most stable electronic state, which is governed by the hole type produced in C_{60}. As can be seen in Table 5.20, the order of the REs of the regioisomers follows the trend of neutral platinum incorporation, which

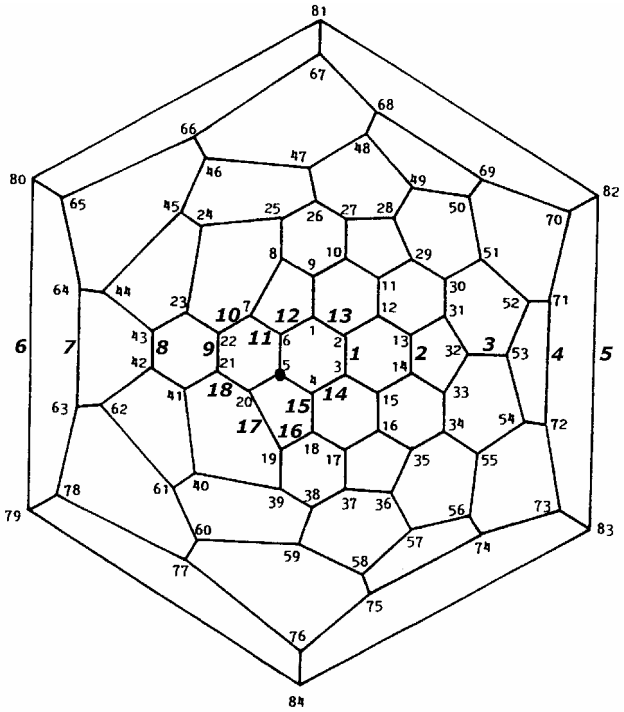

Figure 5.21 Schlegel Diagram showing the numbering system for D_{2d}-C_{84}:**23** fullerene and regioisomers of $C_{81}Pt_2$. See Appendix A.8 for more details in the numbering system of the free D_{2d}-C_{84}:**23**. The small numbers represents C_{84} numbering. At the black dot is situated the tricoordinated-type heteroatom, which substitute the C5 atom. The bigger bold numbers represent the position of the tetracoordinated heteroatom substituting the C–C bond and also the regioisomer number. For instance, the regioisomer $C_{81}Pt_2$:**1** is constructed after the substitution of the C5 atom and C2–C3 bond by two heteroatoms.

confirms the general idea that the most important factor is the destabilization of the carbon cage produced by the incorporation of a metal into the free carbon framework.

*5.5.8 Prediction of isomer stability of $C_{81}Pt_2$, a heterofullerene from D_{2d}-(C_{84}:**23**)*

In the previous sections, we have combined quantum chemistry (DFT) and chemometrics (PLS regression) to analyse and understand the

stabilities of the computed regioisomers of $C_{57}Pt_2$ and $C_{56}Pt_2$. The low prediction error of 0.288 eV for the PLS model of $C_{57}Pt_2$ calculated using only topological factors encouraged us to go further. Since the four topological factors can be estimated a priori, we used PLS regression to predict the stability trends for non-computed structures of the same heterofullerenes or of larger clusters.

In larger fullerenes the complexity may be enormous. Consider for example C_{84}. This fullerene has 24 IPR isomers of which isomer 23 of symmetry D_{2d} has one of the lowest energy similar to those of isomer 22 of symmetry D_2.[41] In this section, we will show that we can use data from heterofullerenes of C_{60} to find relative stabilities for other carbon cages. In particular, we have analysed the substitution of a C_2 unit and a C atom in the D_{2d}-C_{84}:**23** isomer. The resulting $C_{81}Pt_2$ heterofullerene contains a tetracoordinated-type and tricoordinated-type Pt atom which is similar to the situation in $C_{57}Pt_2$. The pyramidalization angle of carbons (θ_p),[42] which is a measure of fullerene sphericity, has not been taken into account in C_{60} because all carbons have the same value however it could be also important. According to Changgeng et al it has an important effect on the regioisomers of $C_{69}M$ –a doped fullerene from C_{70}–, which M replace the most pyramidalized carbon. Pyramidalization angles and bond lengths of all different C–C bonds of D_{2d}-C_{84}:**23** are tabulated in Table 5.21. 18 hypothetical regioisomers of $C_{81}Pt_2$ were built in which the tricoordinated-type heteroatom substitutes the most pyramidalized carbon (C5, θ_p = 10.98°). The second heteroatom substitutes all C–C bonds through the C5–C6 symmetry plane, regioisomers [$C_{81}Pt_2$:**1-9**], and all the C–C bonds which make the Pt–Pt separation less than 3 Å, [$C_{81}Pt_2$:**10-18**] regioisomers (Table 5.21 and Figure 5.21).

The values of the four factors considered for prediction are shown in Table 5.22. Since the geometries were not optimized for regioisomers of $C_{81}Pt_2$, the Pt–Pt separation was estimated from the free C_{60} and C_{84} structures: the tricoordinated heteroatom was placed 0.8 Å above the fullerene surface (like in $C_{59}Pt$) and the tetracoordinated in the middle of the substituted C–C bond. Also for C_{84}, the substituted C–C bond lengths were used instead of C–C bond type due to higher variability in bond lengths in this higher fullerene compared to C_{60}. Because of the different range values of the factors for $C_{57}Pt_2$ and $C_{81}Pt_2$, we could not use the previously

Table 5.21 PLS prediction of isomer stability of $C_{81}Pt_2$, a doped heterofullerene from the D_{2d}-C_{84}:**23** isomer [a]

Iso. Num.	*Subs. C–C bonds* [b]	*Set of C–C bond* [c]	*Pred. RE* [d]	*Calc. RE* [e]	*Pt–Pt* [f]	*No. C–C bonds*	*C–C bond lengths*	*No. Hetero-rings*
18	20,21	7,22	0.000	0.000	2.280	119	1.416	5
14	3,4	1,2	0.041		2.298	119	1.419	5
17	19,20	7,8	0.117		2.164	119	1.428	5
12	1,6	1,6	0.162		2.192	119	1.431	5
15	4,18	1,9	0.317		2.130	119	1.445	5
11	6,7	5,20	0.434		2.200	119	1.453	5
10	7,22	7,22	1.127	0.583	2.952	118	1.416	6
13	1,2	1,2	1.165		2.959	118	1.419	6
16	18,19	8,9	1.368		2.556	118	1.444	6
8	42,43	32,53	1.665		5.371	118	1.375	7
1	2,3	2,3	1.693		3.008	118	1.461	6
9	21,22	21,22	1.771	1.935	2.975	118	1.468	6
3	32,53	32,53	2.254		7.653	118	1.375	7
6	79,80	5,6	2.629		8.731	118	1.377	7
2	13,14	13,14	2.667	2.250	5.401	118	1.456	7
7	63,64	21,22	3.305		7.304	118	1.468	7
4	71,72	13,14	3.554	2.473	8.839	118	1.456	7
5	82,83	2,3	3.670		9.051	118	1.461	7

[a] Distances in Å and energy in eV. The first Pt atom replaces the most pyramidalized carbon (C5, θ_p = 10.98°) and thus it is tricoordinated. The second Pt atom substitutes a C_2 unit and is consequently the tetracoordinated one. So the $C_{81}Pt_2$ heterofullerene shares the same topology as $C_{57}Pt_2$. [b] The substituted C–C bond. See the Appendix A.8 for the numbering system of D_{2d}-C_{84}:**23**. [c] The C–C bond in the previous column belong to this set of C–C bond. The 18 different set of C–C bonds of D_{2d}-C_{84}:**23** are described in Appendix A.8. [d] Predicted from PLS regression model of the four topological factors of $C_{57}Pt_2$ data. [e] DFT calculated relative energy (cal. RE) [f] Non-optimized Pt–Pt separation. The tricoordinated Pt atom is 0.80 Å above the fullerene surface as Pt is in $C_{59}Pt$ whereas the tetracoordinated Pt atom is in the middle of the substituted C–C bond.

calculated regression model. Hence, a PLS model was calculated again from the $C_{57}Pt_2$ data using a different preprocessing. In this case, the four topological factors of $C_{57}Pt_2$ were range-scaled between 0 and 1. The data in Table 5.22 were scaled so that a variation in the scaled variables of $C_{57}Pt_2$ and Table 5.22 corresponded to the same variation in the original *x*-

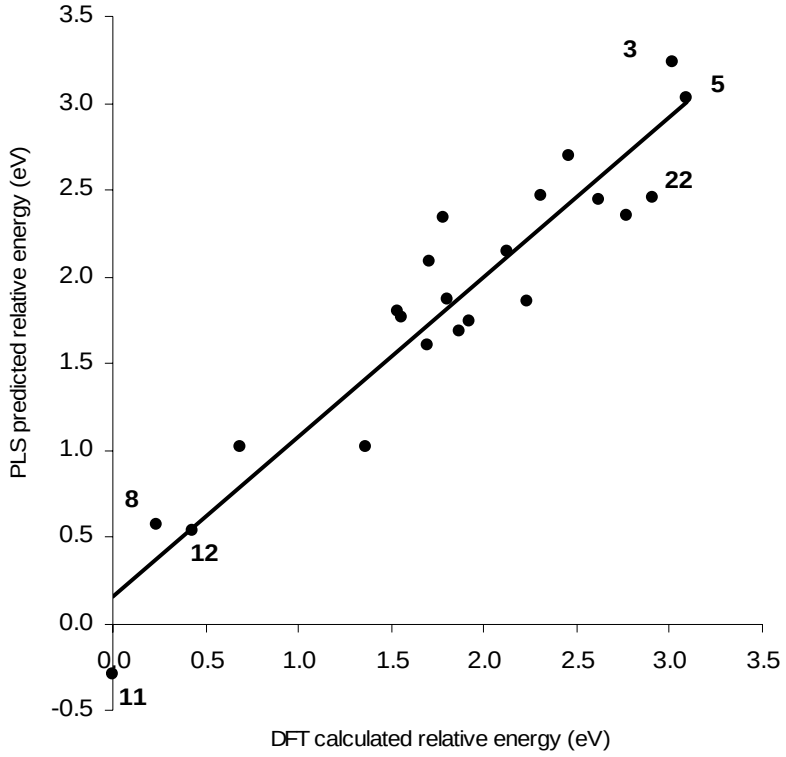

Figure 5.22 DFT calculated versus PLS predicted relative energy (RE) obtained from the PLS regression model on the four topological factors of $C_{57}Pt_2$. Only the most stable and least stable regioisomers are labeled.

variables. The RMSEP of the new PLS model was 0.283 eV, which is similar to the one obtained for autoscaled data hence the different scaling did not reduce the predictive performance of the model. In this case the PLS model represents an 84 % of the original four topological *x*-variables and a 90 % of the relative energy for $C_{57}Pt_2$. The plot of DFT calculated versus PLS predicted REs for this PLS model can be see in Figure 5.22.

The predicted REs are listed in the third column of Table 5.21. Their reliability was tested by comparing the predictions for the representative [$C_{81}Pt_2$:**2**, **4**, **9**, **10** and **18**] regioisomers with the calculated relative energy from the fully optimized DFT geometries. The PLS predicted reliable

relative energy except for $C_{81}Pt_2$:**4** which is the regioisomer with longer Pt–Pt separation and it is an extrapolation for the $C_{57}Pt_2$ PLS model. The mean difference between calculated and predicted for the first three calculated regioisomers was 0.38 eV which is close to the prediction error expected for this model (0.28 eV) so we can consider the PLS predictions as a good indication of the trends in the relative energy to be expected for regioisomers of $C_{81}Pt_2$. All the predictions are consistent with the knowledge acquired about the $C_{56}Pt_2$ and $C_{57}Pt_2$ heterofullerenes. [$C_{81}Pt_2$:**18, 14, 17, 12, 15** and **11**] regioisomers appear as the most stable regioisomers of $C_{81}Pt_2$ because of a short Pt–Pt distance, the high number of retained C–C bonds and fewer heterorings in their structure. Like in $C_{57}Pt_2$ the most stable substitutions are those that distort least the fullerene carbon framework of the D_{2d}-C_{84}:23 fullerene. It is quite probably that the isomer $C_{81}Pt_2$:**18** is not the most stable of all possible structures with formula $C_{81}Pt_2$ but this analysis shows that we have a powerful tool that may help in the study of multiple substitutions in a carbon cage.

5.6 PHYSICAL PROPERTIES

Table 5.23 lists the ionization potentials (IPs) and the electron affinities (EAs) of C_{60}, the monoheterofullerenes C_{2v}-C_{58}M (M = Pt, Ir, Os) and C_{59}M (M = Pt, Ir, Os) and the diheterofullerenes $C_{56}Pt_2$:**10** and $C_{57}Pt_2$:**11** with the corresponding HOMO and LUMO energies. The computed IP and EA of the free C_{60}, 7.56 eV and 2.89 eV, respectively, are in good agreement with the experimental values of 7.6 eV[43] and 2.7 eV[44] estimated from photoelectron spectra. In general, the incorporation of metals in the carbon cage reduces the IP and increases the EA of the cluster. The computed IPs for C_{2v}-C_{58}M were calculated to be 7.37 eV for Pt, 7.06 eV for Ir and 7.41 eV for Os. In the case of C_{59}M, these monoheterofullerenes lose electrons somewhat more readily to form positive ions than C_{2v}-C_{58}M. The EA of C_{60} is increased by doping *ca.* 0.48-0.78 eV for C_{58}M and a little less for C_{59}M (0.09-0.16 eV). Therefore, doping with metals enhanced the redox properties of C_{60}. The changes in the EAs and IPs are easily understood from the relative energies of the HOMO and LUMO. This trend of having somewhat smaller IPs and greater EAs than those of C_{60} has

Table 5.22 Ionization potentials (IPs) and electron affinities (EAs) for several mono- and diheterofullerenes [a]

Molecule	*Sym.*	*IP*	*EA*	*E(HOMO)*	*E(LUMO)*	*HOMO/LUMO gap*
C_{60}	I_h	7.56	2.89	–6.25	–4.59	1.66
$C_{58}Pt$	C_{2v}	7.37	3.67	–5.91	–5.37	0.54
$C_{58}Ir$ [b]	C_{2v}	7.06	3.51	–5.60	–5.26	0.34
$C_{58}Os$	C_{2v}	7.41	3.35	–5.95	–4.96	0.99
$C_{59}Pt$	C_s	6.68	3.05	–5.38	–4.68	0.70
$C_{59}Ir$ [b]	C_s	6.44	3.10	–5.12	–4.82	0.30
$C_{59}Os$	C_s	7.00	2.96	–5.56	–4.64	0.92
$C_{56}Pt_2$:***10***	C_1	7.04	3.64	–5.69	–5.20	0.49
$C_{57}Pt_2$:***11***	C_1	6.78	3.44	–5.53	–5.03	0.50

[a] Values in eV. [b] Energies for the HOMO and LUMO correspond to the energy of the α-single occupied orbital and its β-unoccupied counterpart, respectively.

already been found for Si-,[45] N- and B-doped fullerenes, and metal heterofullerenes such as $C_{59}M$ (M = Fe, Co, Ni and Rh).

For $C_{56}Pt_2$:**10** and $C_{57}Pt_2$:**11** regioisomers, the computed IPs are 7.04 eV and 6.78 eV, respectively, and the corresponding EAs are 3.64 eV and 3.44 eV. Therefore, the incorporation of new metals in the fullerene skeleton of the monoheterofullerenes hardly changes the physical properties of the cluster (Figure 5.23). The same behavior was reported for multiple-substituted $C_{60-x}N_x$ and $C_{60-x}B_x$ heterofullerenes.

5.7 CONCLUDING REMARKS

Mass spectrometric detection. Heterohedral metallofullerenes have only been detected in mass spectrometric studies and so they have not yet been characterized because of the tiny quantities involved. Two main processes have been used to synthesize them. The first method is the photofragmentation of the previously prepared exohedral $C_{60}M_n$ and $C_{70}M_n$ clusters (introduced by Branz). The second alternative route involves the laser ablation of the electrochemically deposited films C_{60}/Pt or C_{60}/Ir(CO)$_2$ (introduced by Balch). Macroscopic synthetic methods have not yet been

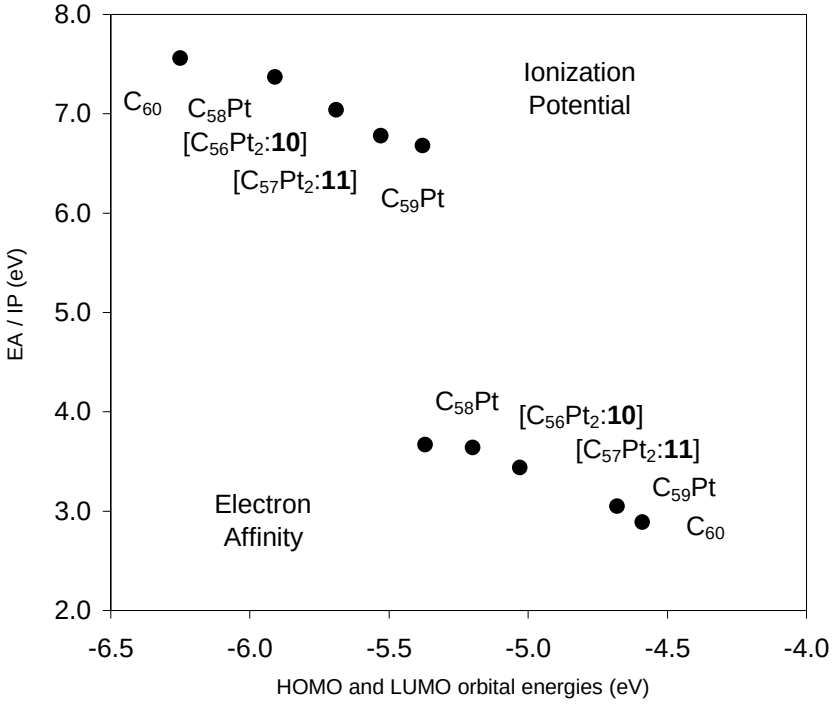

Figure 5.23 Ionizaton potentials (IPs) and electron affinities (EAs) versus HOMO and LUMO energies, respectively, for the free C_{60} and $C_{58}Pt$, $C_{59}Pt$, $C_{56}Pt_2$ and $C_{57}Pt_2$ heterofullerenes.

developed for heterohedral metallofullerenes, although for analogous non-metal heterofullerenes a modified Krästschmer-Huffman process is used satisfactorily. The new metallofullerenes obtained mainly correspond to a C_2 unit or C atom replaced by a metal in C_{60}, yielding the stoichiometries $C_{59}M$ and $C_{58}M$. The diheterofullerenes $C_{57}M_2$ and $C_{56}M_2$ (M = Pt and Ir) are observed when several substitutions occur. A common process observed during the experiments is the successive loss of C_2 units leading to the family of monoheterofullerenes $C_{59-2x}M$ and $C_{58-2x}M$. These last clusters have substantial rearrangements in the fullerene carbon framework, which means that they are more difficult to study than the previous ones.

Geometry and substitution energy (SE). When a metal substitutes a C_2 unit it becomes tetracoordinated. It does not protrude from the fullerene surface but stays within the fullerene carbon framework. This is called substitution energy (SE) which was computed to be 7.35 eV for the most stable isomer of C_{2v}-$C_{58}Pt$, a 6:6 C_2 substitution by a Pt. The other isomer corresponds to a 6:5 C_2 substitution (C_s-$C_{58}Pt.65$), which leads to an isomer that is 0.63 eV less stable. On the other hand, the tricoordinated M atom in $C_{59}M$ protrudes from the fullerene surface because there is not enough space far it to be completely enclosed (SE = 6.20 eV). The SE can be divided into two main contributions: first, the energy necessary to make the hole (hole energy) and, second, the energy involved in inserting the metal into this hole (insertion binding energy, IBE). The hole energy is highly endothermic (17.90 eV for C_{2v}-$C_{58}Pt$ isomer and 19.31 for C_s-$C_{58}Pt.65$) and determines the relative stability of the two isomers. The 6:6 C–C substitution is more favorable than the 6:5 C–C substitution because the former involves the destruction of fewer π C–C bonds. On the other hand, the IBE is an exothermic process that is slightly more favorable for the 6:5 substitution (−10.55 eV for C_{2v}-$C_{58}Pt$ and −11.33 eV for C_s-$C_{58}Pt$). However, the IBE is not capable of overcoming the greater destabilization produced in the 6:5 isomer during the hole-making process.

Metal covalent bond within the fullerene carbon framework. According to the fragment molecular orbital method, the Pt atom in the C_{2v}-$C_{58}Pt$ isomer has 18 electrons involved in the metal-carbon bond (4 σ sp^2, 4 π p_z and 10 *d*-based electrons) in the 0 oxidation state. We have used the D_{4h}-$C_{24}H_{12}Pt$ heterocompound as a feasible model for the C_{2v}-$C_{58}Pt$ monoheterofullerene, which can be taken as a general example of the metal insertion in heterofullerenes. In the D_{4h}-$C_{24}H_{12}Pt$ heterocompound, the metal-carbon bond can be separated into two contributions: σ and π. In general, the metal-carbon bond consists of two σ and two π interactions. The interaction between the sp^2 carbon ligand orbitals of the four dangling C with the d_z^2 and d_{xy} metal orbitals provides the two σ bonds. The π bond is formed through the interaction between the p_z carbon ligand orbitals and the d_{xz} and d_{yz} metal orbitals. The d_{x2-y2} metal orbital has a non-bonding character. These model bonding orbitals are slightly modified in the C_{2v}-$C_{58}M$ heterofullerene in the sense that σ and π molecular orbitals (MOs) are

allowed to mix but they retain all the main bonding characteristics of the MOs described above for the D_{4h}-$C_{24}H_{12}Pt$ heterocompound. To sum up, the highly exothermic and favorable process of the metal insertion, *ca.* –11 eV for 4 Pt–C bonds, is confirmed by the presence of four covalent metal-carbon bonding MOs.

Stability of monoheterofullerenes. $C_{58}M$ and $C_{59}M$ (M = Ir, Os, Ti) exhibit the same inertion pattern as $C_{58}Pt$ and $C_{59}Pt$. The 6:6 C_2 substitution is much easier (*ca.* 0.6 eV for all studied isomers) than the 6:5 C_2 substitution. Another conclusion is that the insertion of larger metals such as Os and Ir is favoured because they cause less cage deformation. The difference between Pt and Os incorporations is of *ca.* 2 eV. Particularly important is the correlation between the geometric parameters (cage radius and HOMA) and the substitution energy (SE): small cage radius and high HOMA values are accompanied by lower SE values, which indicates that the deformation of the cage caused by the metal insertion is essential to the stabilization of the heterofullerenes. As expected, the substitution of one C atom by a metal is a little bit more favorable (*ca.* 1 eV). It is also important to notice that the SE is significantly reduced when the cation or anion of these heterofullerenes is used, thus facilitating the formation process.

Ethylene addition, a proof of heterofullerenes. The experimental detection of substrates such as 2-butene added to the heterofullerenes $C_{58}M$ and $C_{59}M$ has confirmed the heterohedral position of the metal in these metallofullerenes. The ethylene coordinates to the metal without disrupting the fullerene structure at long M–C distances: for example, 2.447 Å for $C_{58}Pt(C_2H_4)$ compared to 2.148 Å for $(\eta^2\text{-}C_2H_4)Pt(PH_3)_2$ complexes. The binding energy (BE) is –0.70 eV for $C_{58}Pt(C_2H_4)$ and the partitioning scheme of the BE indicates that the orbital term is clearly dominated by the σ donation, instead of the π back-donation which occurs in the $(\eta^2\text{-}C_2)Pt(PH_3)_2$ complexes. In other words, the ligand to metal σ donation is more effective than the metal to ligand π back-donation at long M–ethylene distances. The geometry and the BE change significantly for the reduction and oxidation processes of these coordinated heterofullerenes.

Stability of polyheterofullerenes. When two Pt atoms replace two C_2 units, or one C_2 unit and one C atom in C_{60}, a priori, multiple regioisomers are possible. Calculations carried out on numerous regioisomers of $C_{57}Pt_2$ and $C_{56}Pt_2$ clearly show that the metals occupy neighbouring positions in the most stable structures. Metal substitution deforms the fullerene carbon framework and partially destroys the fullerene aromaticity. This is the *key* factor in determining the stability of these disubstituted clusters. Indeed, it is much easier to make a big hole that permits the incorporation of two Pt atoms in the carbon cage than two smaller holes in two opposite sites of the fullerene. The structures with two neighbouring Pt atoms retain the greatest number of C–C bonds; this aspect is another important factor that determines the stability of the cluster. In addition, clusters with short Pt–Pt contacts may contain weak metal-metal interactions, which also favour the stability of the cluster but which are not a fundamental stability element. The 6:6 substitutions are preferred to the 6:5 substitutions, as we have seen in monoheterofullerenes. In our opinion, these results go beyond the particular cases of the $C_{57}Pt_2$ and $C_{56}Pt_2$ regioisomers and we believe that the present conclusions can be extended to any transition metal derivative. Calculations performed on the ionic species of the Pt-derivatives and on some Ti homologues confirm the hypothesis that disubstituted C_{60} fullerenes should contain the heteroatoms in adjacent sites. The behavior of larger fullerenes such as C_{70} should be similar although in this case the curvature of the fullerene could also be important, as previously shown in monosubstituted species.

Chemometric tools. Partial least squares (PLS) was the technique satisfactorily used to analyze the interdependencies among all the factors that govern the stability of these diheterofullerene clusters. We conclude that no factor by itself is capable of explaining the relative stability but that the combination of topological factors such as Pt–Pt separation, number of C–C bonds, substituted C–C bond type and number of heterorings can satisfactorily describe the general trends of the relative stability. Although the curvature and the increase in the cage can affect isomer stability, we have been able to predict the trends of the REs of the regioisomers of $C_{81}Pt_2$, a doped fullerene from the free D_{2d}-C_{84}:**23** fullerene. We used a PLS regression model from the analogous $C_{57}Pt_2$ data to predict the stability of

the $C_{81}Pt_2$ heterofullerene. This is probably our greatest contribution to metallofullerene research.

Physical properties. Doping with metals enhanced the redox properties of C_{60}: smaller ionization potentials and higher electron affinities are found for the heterohedral metallofullerenes. However, the incorporation of new metals in the fullerene skeleton of the monoheterofullerenes hardly changes the physical properties of the clusters.

REFERENCES AND NOTES

[1] Krätschmer, W.; Lamb, L. D.; Fostiropoulos, K.; Huffman, D. *Nature* **1990**, *347*, 354. Muhr, H. J. ; Nesper, R. ; Banhart, F. ; Zwanger, M. *Abstract, International Winterschool on Electronic Properties of Novel Materials : Fullerides and Fullerols*, **1995**, Tyrol.

[2] Clemmer, D. E.; Hunter, J. M.; Shelimov, K.B.; Jarrold, M. F. *Nature* 1994, *372*, 248. Shelimov, K. B.; Clemmer, D. E.; Jarrold, M. F. *J. Phys. Chem.* **1994**, *98*, 12819.

[3] Branz, W.; Billas, I.M. L.; Malinowski, N.; Tast, F.; Heinebrodt, M.; Martin, T. P. *J. Chem. Phys*. **1998**, *109*, 3425.

[4] Billas, I. M. L.; Branz, W.; Malinowski, N.; Tast, F.; Heinebrodt, M.; Martin, T. P.; Massobrio, C.; Boero, M.; Parrinello, M. *NanoStruct. Mat.* **1999**, *12*, 1071.

[5] Poblet, J. M.; Muñoz, J.; Winkler, K.; Cancilla, M.; Hayashi, A.; Lebrilla, C. B.; Balch, A. L. *Chem. Comm.* **1999**, 493.

[6] Balch, A. L.; Costa, D. A.; Winkler, K. *J. Am. Chem. Soc.* **1998**, *120*, 9614.

[7] Hayashi, A.; de Bettencourt-Dias, A; Winkler, K.; Balch, A. L. *J. Mater. Chem.* **2002**, *12*, 2116.

[8] Kong, Q.; Shen, Y.; Zhao, L.; Zhuang, J.; Qian, S.; Li, Y.; Lin, Y.; Cai, R. *J. Chem. Phys.* **2002**, *116*, 128.

[9] Hayashi, A.; Xie, Y.; Poblet, J. M.; Campanera, J. M.; Lebrilla, C. L.; Balch, A. L. *J. Phys. Chem. A* **2004**, *108*, 2192.

[10] Hirsch, A.; Nuber, B. *Acc. Chem. Res*.**1999**, *32*, 795; Chen, Z.; Ma, K.; Chen, L.; Zhao, H.; Pan, Y.; Zhao, X.; Tang, A.; Feng, J. *J. Mol. Struc. (Theochem)* **1998**, *452*, 219.

[11] Chen, Z.; Zhao, X.; Tang, A. *J. Phys. Chem. A* **1999**, *10*3, 10961.

[12] Chen, Z; Reuther, U.; Hirsch, A.; Thiel, W. *J. Phys. Chem A* **2001**, *105*, 8105.

[13] Jiao, H.; Chen, Z.; Hirsch, A.; Thiel, W. *Phys. Chem. Chem. Phys.* **2002**, *4*, 4916.

[14] Turker, L. *J. Mol. Struc. (Theochem)* **2002**, *593*, 149.

[15] Jiao, H.; Chen., Z. Hirsch, A. Thiel, W. *J. Mol. Mod.* **2003**, *9*, 34.
[16] Billas, I. M. L.; Massobrio, C.; Boero, M.; Parrinello, M.; Branz, W.; Tast, F.; Malinowski, N.; Heinebrodt, M.; Martin, T. P. *J. Chem. Phys.* **1999**, *111*, 6787.
[17] Ding, C. G.; Yang, J. L.; Cui, X. Y.; Chan, C. T. *J. Chem. Phys.* **1999**,*111*, 8481.
[18] Ding, C. G.; Yang, J. L.; Han, R.; Wang, K. *Physical Review A* **2001**, *64*, 43201.
[19] Billas, I. M. L.; Massobrio, C.; Boero, M.; Parrinello, M.; Branz, W.; Tast, F.; Malinowski, N.; Heinebrodt, M.; Martin, T. P. *Comput. Mat. Sci.* **2000**, *17*, 191.
[20] Kong, Q.; Zhuang, J.; Xu, J.; Shen, Y., Li, Y. ; Zhao, L.; Cai, R. F. *J. Phys. Chem A* **2003**, 107, 3670.
[21] (a) Ziegler, T.; Rauk, A. *Teor. Chim. Acta* **1977**, *46*, 1. (b) *Inorg. Chem.* **1979**, *18*, 1558.
[22] (a) Morokuma, K. *J. Chem. Phys.* **1971**, *55*, 1236. (b) Kitaura, K.; Morokuma, K. *Int. J. Quantum. Chem.* **1976**, *10*, 325.
[23] Albright, T. A. *Tetrahedron* **1982**, *38*, 1339.
[24] (a) Kruszewski, J.; Krygowski, T. M. *Tetrahedron Lett.* **1972**, *3839*. (b) Krygowski, T. M. *J. Chem. Inf. Comput. Sci.* **1993**, *33*, 70.
[25] Krygowski, T. M.; Cyranski, M. K. *Chem. Rev.* **2001**, *101*, 1385.
[26] Fowler, P.W.; Manoloupoulus, D. E. *An Atlas of Fullerens*, Oxford University Press, Oxford, **1995**.
[27] (a) Restivo, R. J.; Ferguson, G.; Kelly, T. L.; Senoff, C. V. *J. Organomet. Chem*. **1975**, *90*, 101. (b) Koster, R.; Seidel, G.; Kruger, C.; Muller, G.; Jiang, A.; Boese R. *Chem. Ber.* **1989**, *122*, 2075. (c) Lundquist, E. G.; Folting, K.; Huffman, J. C.; Caulton, K. G. *Organometallics* **1990**, *9*, 2254. (d) Wakefield, J. B.; Stryker, J. M. *Organometallics* **1990**, *9*, 2428**.** (e) Einstein, F. W. B.; Yan, X.; Sutton, D. *Chem.Commun.* **1990**, 1466. (f) Lundquist, E. G.; Folting, K.; Streib, W. E.; Huffman, J. C.; Eisenstein, O.; Caulton, K. G. *J. Am. Chem. Soc.* **1990**,*112*, 855. (g) Bell, T. W.; Helliwell, M.; Partridge, M. G.; Perutz, R.N. *Organometallics* **1992**, *11*, 1911. (h) Burger, P.; Bergman, R. G. *J. Am. Chem. Soc.* **1993**, *115*, 10462. (i) Huffer, S.; Wieser, M.; Polborn, K.; Beck, W. *J. Organomet. Chem.* **1994**, *481*, 45. (j) Batchelor, R. J.; Einstein, F. W. B.; Lowe, N. D.; Palm, B. A.; Yan, X.; Sutton, D. *Organometallics* **1994**, *13*, 2041. (k) Cleary,B. P.; Eisenberg, R. *J. Am. Chem. Soc.* **1995**, *117*, 3510. (l) Aizenberg, M.; Milstein, D.; Tulip, T. H. *Organometallics* **1996**, *15*, 4093. (m) Alvarado, Y.; Boutry, O.; Gutierrez, E.; Monge, A.; Nicasio, M. C.; Poveda, M. L.; Perez, P. J. Ruiz, C.; Bianchini, C.; Carmona, E. *Chem. Europ. J.* **1997**, *3*, 860. (n) Antwi-Nsiah, F. H.; Torkelson, J. R.; Cowie, M. *Inorg. Chim. Acta* **1997**, *259*, 213. (o) Gutierrez-Puebla, E.; Monge, A.; Nicasio, M. C.; Perez, P. J.; Poveda, M. I.; Rey, L.; Ruiz, C.; Carmona, E. *Inorg. Chem*. **1998**, *37*, 4538. (p) Slugove, C.; Mereiter, K.; Trofimenko, S.; Carmona, E. *Chem. Commun.*

2000, 121. (q) Wiley, J. S.; Oldham, Jr., W. J.; Heinekey, D. M. *Organometallics*, **2000**, *19*, 1670.
[28] Nunzi, F.; Sgamelloti, A.; Re, N.; Floriani, C. *Organometallics* **2000**, *19*, 1628.
[29] (a) Cheng, P.-T.; Nyburg, S. C. *Can. J. Chem.* **1972**, *50*, 912. (b) Burns, C. J.; Andersen, R. A. *J. Am. Chem. Soc.* **1987**, *109*, 915. (c) Clark, H. C.; Ferguson, G.; Hampden-Smith, M. J.; Kaitner, B.; Ruegger, H. *Polyhedron* **1988**, *7*, 1349. (d) Camalli, M.; Caruso, F.; Chaloupka, S.; Leber, E. M.; Rimml, H.; Venanzi, L. M. *Helv. Chim. Acta* **1990**, *73*, 2263. (e) Mole, L.; Spencer, J. L.; Carr, N.; Orpen, A. G. *Organometallics* **1991**, *10*, 49. (f) Fulwood, R.; Parker, D.; Ferguson, G.; Kaltner, B. *J. Organomet. Chem.* **1991**, *419*, 269. (g) Baker, M. J.; Harrison, K. N.; Orpen, A. G.; Pringle, P. G.; Shaw, G. *J. Chem. Soc., Dalton Trans.* **1992**, 2607.
[30] Dedieu, A *Chem. Rev.* **2000**, *100*, 543.
[31] Frenking, G.; Frölich, N. *Chem.Rev.* **2000**, *100*, 717.
[32] (a) Fagan P. J.; Calabrese, J. C.; Malone, B. *J. Am. Chem. Soc.* **1991**, *113*, 9408. (b) Fagan, P. J.; Calabrese, J. C.; Malone, B. *Acc. Chem. Res.* **1992**, *25*, 134. (c) Balch, A. L.; Lee, J. W.; Noll, B. C.; Olmstead, M. M. *J. Am. Chem. Soc.* **1992**, *114*, 10984. (d) Bo, C.; Costas, M.; Poblet, J. M. *J. Phys. Chem*. **1995**, *99*, 5914.
[33] Allen, F. H. *Acta Crystallogr.* **B58**, 380-388, 2002.
[34] Alcock, N. W.; Bergamini, P.; Gomes-Carniero, T. M.; Jackson, R. D.; Nicholls, J.; Orpen, A. G.; Pringle, P. G.; Sostero, S.; Traverso, O. *J. Chem. Soc., Chem.Commun.* **1990**, *4*, 980.
[35] (a) Bader, R. W. F. Atoms in Molecules, A Quantum Theory, Clarendon Press: Oxford, U.K., **1990**. (b) Bader, R. W. F., MacDougall, P. J.; Lau, C. D. H. *J. Am. Chem. Soc.* **1984**, *106*, 1594.
[36] Bénard, M.: Rohmer, M. M.; Poblet, J. M. *Chem. Soc. Rev.* **2000**, *100*, 495.
[37] (a) Kurita, N.; Kobayashi, K.; Kumabora, H.; Tago, K. *Phys. Rev. B* **1993**, *48*, 4850. (b) Kurita, N.; Kobayashi, K.; Kumabora, H.; Tago, Ozawa, K. *Chem. Phys. Lett.* **1992**, *198*, 95. (c) Kurita, N.; Kobayashi, K.; Kumabora, H.; Tago, K. *Fullerene Sci. Technol.* **1993**, *1*, 319.
[38] Chen, Z.; Ma, K.; Pan, Y.; Zhao, X.; Tang, A.; Feng, J. *J. Chem. Soc., Faraday Trans.* **1998**, *94*, 2269.
[39] (a) Poater, J.; Fradera, X.; Duran, M.; Solà, M. *Chem. Eur. J.* **2003**, *9*, 5. (b) Poater, J.; Fradera, X.; Duran, M.; Solà, M. *Chem. Eur. J.* **2003**, *9*, 2.
[40] Massart, D. L.; Vandeginste, B. G. M.; Buydens, L. M. C.; De Jong, S.; Lewi, P. J.; Smeyers-Verbeke, J. *Handbook of Chemometrics and Qualimetrics*; Elsevier Science: Amsterdam, 1998; Parts A and B.
[41] (a) Fowler, P. W.; Manolopoulos, D. E. *An Atlas of Fullerenes*, Oxford, **1995**. (b) Zhang, B. L.; Wang, C. Z.; Ho, K. M. *J. Chem. Phys.* **1992**, *96*, 7183. (c) Wang,

X. Q.; Wang, C. Z.; Zhang, B. L.; Ho, K. M. *Phys. Rev. Lett.* **1992**, *69*, 69. (d) Wang, X. Q.; Wang, C. Z.; Zhang, B. L.; Ho, K. M. *Chem. Phys. Lett.* **1993**, *207*, 349.

[42] (a) Haddon, R. C.; Scott, L. T. *Pure Appl. Chem.* **1986**, *58*, 137. (b) Haddon, R. C. *J. Am. Chem. Soc.* **1986**, *108*, 2837. (c) Haddon, R. C.; Chow, S. Y. *J. Am. Chem. Soc.* **1998**, *120*, 10494.

[43] Lichtenberger, D. L.; Nebesny, K. W.; Ray, C. D.; Huffman, D. R.; Lamb, L. D. *Chem. Phys. Lett.* **1991**, 176, 203.

[44] Yang, S. H.; Pettiette, C. L.; Concienciao, J.; Cheshnowsky, O. ; Smalley, R.E. *Chem. Phys. Lett.* **1991**, *139*, 233.

[45] Lu, J.; Luo, Y.; Huang, Y.; Zhang, X.; Zhao, X. *Solid State Comm.* **2001**, *118*, 309.